AD-A080 066 FORD AEROSPACE AND COMMUNICATIONS CORP NEWPORT BEACH --ETC F/G 20/4
TRANSITION TO TURBULENCE IN FREE SHEAR-LAYERS.(U)
OCT 79 A DEMETRIADES F44620-75-C-0016
UNCLASSIFIED U-6573 AFOSR-TR-80-0056 NL

| OF |
ADA
080066

END
DATE
FILMED
2-80
DDC

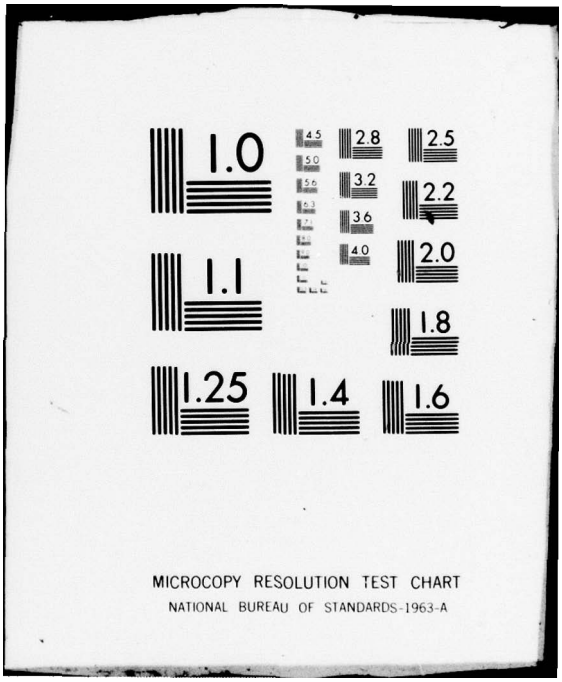
1.0
1.1
1.25
1.4
1.6
1.8
2.0
2.2
2.5
2.8
3.2
3.6
4.0
4.5
5.0
5.6
6.3
7.1
MICROCOPY RESOLUTION TEST CHART
NATIONAL BUREAU OF STANDARDS-1963-A

[redacted]

AFOSR-TR- 80-0056

FACC PUBLICATION NO. U-6573

LEVEL II

12

TRANSITION TO TURBULENCE IN FREE SHEAR LAYERS

by
A. Demetriades
Ford Aerospace & Communications Corp.
Aeronutronic Division
Ford Road
Newport Beach, California

Work Performed for

Air Force Office of Scientific Research
Building 410
Bolling Air Force Base
Washington, D.C. 20332

Under Contract

AFOSR F44620-75-C-0016

October 1979

FINAL

Approved for Public Release; Distribution Unlimited

SECURITY CLASSIFICATION OF THIS PAGE (When Data Entered)

REPORT DOCUMENTATION PAGE	READ INSTRUCTIONS BEFORE COMPLETING FORM
1. REPORT NUMBER: AFOSR-TR-80-0056	2. GOVT ACCESSION NO. / 3. RECIPIENT'S CATALOG NUMBER
4. TITLE (and Subtitle): TRANSITION TO TURBULENCE IN FREE SHEAR-LAYERS	5. TYPE OF REPORT & PERIOD COVERED: FINAL rept. Oct 74 — Oct 79
	6. PERFORMING ORG. REPORT NUMBER: U-6573
7. AUTHOR(s): A. DEMETRIADES	8. CONTRACT OR GRANT NUMBER(s): F44620-75-C-0016
9. PERFORMING ORGANIZATION NAME AND ADDRESS: FORD AEROSPACE AND COMMUNICATIONS CORPORATION, AERONUTRONIC DIVISION, NEWPORT BEACH, CA 92663	10. PROGRAM ELEMENT, PROJECT, TASK AREA & WORK UNIT NUMBERS: 2307 A2
11. CONTROLLING OFFICE NAME AND ADDRESS: AIR FORCE OFFICE OF SCIENTIFIC RESEARCH/NA, BLDG 410, BOLLING AIR FORCE BASE, D C 20332	12. REPORT DATE: Oct 79 / 13. NUMBER OF PAGES: 77
14. MONITORING AGENCY NAME & ADDRESS (if different from Controlling Office)	15. SECURITY CLASS. (of this report): UNCLASSIFIED / 15a. DECLASSIFICATION/DOWNGRADING SCHEDULE

16. DISTRIBUTION STATEMENT (of this Report)

Approved for public release; distribution unlimited.

17. DISTRIBUTION STATEMENT (of the abstract entered in Block 20, if different from Report)

18. SUPPLEMENTARY NOTES

19. KEY WORDS (Continue on reverse side if necessary and identify by block number)

FREE SHEAR LAYER
TRANSITION
TURBULENCE
SUPERSONIC
TURBULENT WAKES
DENSITY FLUCTUATIONS

20. ABSTRACT (Continue on reverse side if necessary and identify by block number)

Part I of this report presents an investigation of the transition to turbulence in free shear layers. A theoretical analysis is performed to drive a formula for predicting transition, based on the novel approach used earlier by the same investigators to predict transition in wakes and boundary layers. The formula so derived shows that the transition Reynolds number increases as the non-dimensional velocity ratio decreases, and also as the "fast side" Mach number and "slow side" total temperature are increased. An experiment to test the theory was performed; together with earlier transition data, the new data provide good -

→ next page

DD FORM 1 JAN 73 1473

UNCLASSIFIED

SECURITY CLASSIFICATION OF THIS PAGE (When Data Entered)

391853

support for the theory. However, a strong dependence of the transition Reynolds number on unit Reynolds number characterizes the available data, whereas the theory does not predict such dependence. In Part II of this report a brief account is given on the measurement of temperature fluctuations in a cooled compressible turbulent wake. The results endorse the novel detection technique utilized, and support theoretical predictions made earlier under this contract.

Qualified requestors may obtain additional copies from the Defense Documentation Center, all others should apply to the National Technical Information Service.

FOREWORD

The work reported herein concludes research performed at the Aeronutronic Division, Ford Aerospace & Communications Corporation, on fluid-mechanic problems involving stability, transition and turbulence in high-speed shear layers and adjacent streams under USAFOSR Contract F44620-75-C-0016. During the period of this Contract a number of significant experiments were done on the hydrodynamic stability of hypersonic boundary layers, resulting in a significant fraction of the existing data on boundary-layer stability with and without wall cooling. Theoretical and experimental work was also done in setting up rules for predicting wake behavior in gas-dynamic-laser cavities. More recently the effort concentrated in formulating a general transition theory for all parallel shear flows. The latter topic is the subject of this report.

The work reported here deals with the formulation of the theory specifically for free shear layers, and was supported by the Air Force weapons Laboratory, Kirtland AFB, N.M. (Dr. P. J. Ortwerth). The program is directed by the U.S. Air Force Office of Scientific Research (Col. Lowell Ormand), Bolling AFB, Washington, D.C. The wind-tunnel tests were performed at AEDC, Tallahoma, Tenn., at the request of the U.S. Air Force Space and Missile Systems Organization (SAMSO/RSSE, Maj. M. Sabin). Mr. J. Donaldson of ARO, Inc., was the wind-tunnel project engineer. Principal investigator at Aeronutronic was Dr. A. Demetriades from October 1978 until May 1979. Dr. A. J. Laderman was responsible for the program from June until September 1979, during which time he contributed material for inclusion in this report.

Part I of this report presents the shear-layer project, while Part II presents briefly a test done in Aeronutronic's supersonic wind-tunnel on supersonic turbulent wakes. The list of symbols and Figure captions, as well as the References and Figures for both Parts I and II are grouped together in the beginning and the end of this report respectively, and are numbered sequentially for that purpose.

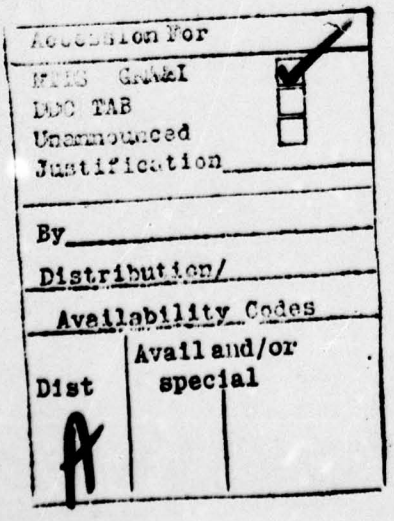

ABSTRACT

Part I of this report presents an investigation of the transition to turbulence in free shear layers. A theoretical analysis is performed to drive a formula for predicting transition, based on the novel approach used earlier by the same investigators to predict transition in wakes and boundary layers. The formula so derived shows that the transition Reynolds number increases as the non-dimensional velocity ratio decreases, and also as the "fast side" Mach number and "slow side" total temperature are increased. An experiment to test the theory was performed; together with earlier transition data, the new data provide good support for the theory. However, a strong dependence of the transition Reynolds number on unit Reynolds number characterizes the available data, whereas the theory does not predict such dependence. In Part II of this report a brief account is given on the measurement of temperature fluctuations in a cooled compressible turbulent wake. The results endorse the novel detection technique utilized, and support theoretical predictions made earlier under this contract.

TABLE OF CONTENTS

TABLE OF CONTENTS (cont'd.)

LIST OF SYMBOLS

A:	A constant in the transducer calibration
B:	A constant in the transducer calibration
b:	Wake width
C:	A constant in the transition formula (see Equation (11))
c_1:	A constant connecting integral scale with FSL width
c':	A constant in an earlier transition formula
DSL:	Dividing streamline
f:	Frequency
FSL:	Free shear layer
$f(M_1)$:	A function of M_1 (see Equation (A.3))
$g(M_1)$:	A function of M_1 (see Equation (6))
h:	The FSL width
k:	The temperature-viscosity exponent
M:	Mach number
p:	Pressure
P_T:	Pitot pressure
Re':	Unit Reynolds number
Re_{XT}:	Transition Reynolds number
Re_Λ:	Turbulence Reynolds number
Re_{Λ_o}:	Critical value of Re_Λ, a constant
T:	Temperature
u:	Velocity
x:	Distance from the FSL origin
X_T:	Location of transition

SYMBOLS (cont'd.)

α_1: The first deflection of the flow (angle of attack of model)

α_2: The second flow deflection (wedge or ramp angle)

γ: Specific heat ratio

$\Gamma(M_1)$: A function of M_1 (see Equation (9))

η: Transverse flow coordinate

λ: Velocity ratio $= \dfrac{u_1 - u_2}{u_1 + u_2}$

Λ: Integral scale

υ: Kinematic viscosity

ρ: density

σ_o: Spreading parameter

$(\ )_1$: Quantities on faster side of FSL

$(\ )_2$: Quantities on slow side of FSL

$(\ )_o$: Supply conditions

$(\ )_\infty$: Stream conditions

$(\ )_w$: Wall conditions

$(\ )_{DSL}$: Conditions on dividing streamline

$(\ )'$: Fluctuation

$\Delta(\ )$: Time-dependent component

FIGURE CAPTIONS

FIGURE CAPTIONS (cont'd.)

PART I
TRANSITION IN FREE SHEAR LAYERS

1.1 INTRODUCTION

The author of this report has devised a method of predicting transition to turbulence in shear flows such as wakes, jet, boundary layers and free shear layers. The method is based on simple but indisputable physical principles, and thus constitutes a necessary condition for the occurence of transition. Since no empiricism is involved, there are no "adjustable constants"; the constants appearing are well-defined physical properties, even though not always known accurately in a numerical sense. The theory has had notable success in wake flows (Reference 1) as well as in boundary layers (Reference 2).

Application of this approach to free shear layers (FSL) is needed, since the forecast of transition in an FSL is the first step in mixing process calculations. The practical incentive for this work was the necessity to predict the flow in chemical laser and gas-dynamic laser cavities, where such mixing is generated. There is, however, a more important objective: a general method of transition prediction for any type of shear flow, explicitly including effects of geometry, compressibility, etc. is an ideal situation because it can be applied quickly and with confidence. It was felt that the past success of this technique in wakes and boundary layers already hinted at such generality. If successful in shear layers as well, the method could indeed represent a big step in solving the long-vexing problem of transition to turbulence.

The past knowledge on FSL transition had been summarized by Birch and Keyes (Reference 3, Figure 2). Progress seems to have stopped at the definition of the "transition parameter" Re_{XT} λ and the empirical finding that this parameter increases with M_1. In other words, all we knew was that the transition zone (a) scaled as Re_{XT}, (b) moved downstream as λ decreased, and as M_1 increased. Indicated improvements were the formation of a rational theory, as well as the generation of more experimental data. The present work deals with these two issues.

Beside the formation of the theory, the present work supplies new experimental data on FSL transition. The experiment was performed in the AEDC Tunnel B at hypersonic speeds although the M_1 levels were only supersonic. The so-called velocity ratio, λ, was very small (of order 0.05) and this, together with the Mach numbers achieved ($3 < M_1 < 4$), represented a regime previously unexplored in FSL transition research. The data, joined by the few earlier sets of data available, will be in due course compared with the theory, which will be first presented below.

1.2 TRANSITION PREDICTIONS

1.2.1 METHOD

The theoretical approach to predicting transition in the FSL is the same as utilized earlier by Demetriades (References 1 and 2) for deriving analogous equations for the wake and boundary layer. The central statement of this method is that the turbulence Reynolds number

$$Re_\Lambda = \frac{u'\Lambda}{\upsilon} \tag{1}$$

in the downstream portion of the turbulent flow following the transition tone, has to have a minimum value Re_{Λ_o}. The mechanics of prediction then consist, first, of assuming that the particular flow under scrutiny is wholly turbulent; then, Re_Λ is computed along this hypothetically turbulent flow. The point along the flow where Re_Λ equals Re_{Λ_o} is the transition point, upstream of which Re_Λ is usually smaller than Re_{Λ_o}. Since no turbulent flow can exist unless $Re_\Lambda > Re_{\Lambda_o}$, this upstream region is laminar.

Thus, according to the above, the present task consists of computing the turbulence Reynolds number, given by Equation (1), along the FSL. This means that the fluctuation intensity u', scale length Λ and kinematic viscosity υ should be computed as a function of the distance x from the flow origin, going downstream. Before this computation is done below, however, *it is necessary to clarify, or at least discuss,* the following conceptual difficulty., The quantity Re_Λ varies across the layer as well as with x, and since u' is zero outside the FSL and has a maximum in it, then Re_Λ will also have a maximum in it according to its definition (Equation (1)). The question now is, what value of Re_Λ is to be chosen at each x. If we choose the maximum Re_Λ, then we imply that the flow can locally sustain the turbulence if Re_Λ reaches Re_{Λ_o} at that point only. This is clearly awkward: assume, for example, that $Re_\Lambda = Re_{\Lambda_o}$ at the center of the flow section; turbulence will then only be permitted in the exact center of the flow and not anywhere else. Strictly speaking this is an inadmissible claim.

In parallel work done by this writer to investigate transition in a boundary layer, the same question could not be circumvented, and the theory had to consider the lateral variation of Re_Λ at each x station. On the other hand, in applying the theory to wakes (Reference 1), successful predictions were made using the Re_Λ magnitude in the center of the flow. Therefore, despite the misgivings of the preceding paragraph, we will here take the following position: if a turbulent FSL has a maximum Re_Λ equal to or larger than the threshold Re_{Λ_o}, then that flow is permitted to be locally turbulent. If, however, conditions are such that Re_Λ at its maximum is below Re_{Λ_o}, turbulence is forbidden. Transition will lie at the boundary between the permitted and forbidden portions of the FSL.

This postulate now clears the way for computing a unique Re_Λ (x) for each given FSL. We know that u' will have a maximum on the dividing

streamline (DSL); thus, all quantities in Equation (1) must be computed there.

1.2.2 CALCULATION OF THE TURBULENCE REYNOLDS NUMBER

The objective now is to compute the variation of Re_Λ for any shear layer, allowing for a wide variation of the FSL conditions such as M_1, λ and T_{02}/T_{01} (no gas composition differences are considered here; only homogeneous flows are discussed). In line with previous remarks, only the Re_Λ along the dividing streamline will be computed. Thus, for each FSL, a unique curve Re_Λ (x) will be obtained; the point where $Re_\Lambda = Re_{\Lambda_o}$ will be the "transition point". Thus, the transition distance will be expressed in terms of the FSL parameters:

$$x_T = x_T \left(M_1, \lambda, \frac{T_{02}}{T_{01}}\right) \tag{2}$$

and some constants which will be discussed in due course. The parameters forming Re_Λ in Equation (1) will now be evaluated one by one.

1.2.2.1 Kinematic Viscosity

The subscript convenction will be to use "1" for the faster and "2" for the slower stream, and no subscript at all for properties on the dividing streamline (or "DSL"). Thus,

$$\upsilon = \left(\frac{T}{T_1}\right)^{k+1} \upsilon_1 \tag{3}$$

where k, the temperature-viscosity exponent, is about 0.75 for air. The temperature ratio in this equation can then be found in the Appendix:

$$\frac{T}{T_1} = \frac{1}{2}\left(1 + \frac{\gamma - 1}{2} M_1^2\right)\left(1 + \frac{T_{02}}{T_{01}}\right) - \frac{(\gamma - 1) M_1^2}{2(1 + \gamma)^2} \tag{4}$$

1.2.2.2 Integral Scale

The integral scale Λ is perhaps the least known of the quantities needed; in contrast with the Crocco relation giving Equation (4), above, the scale comes largely from making an educated guess. This is that (a) Λ is constant across the FSL width and (b) Λ is proportional to the width:

$$\Lambda = c_1 h \tag{5}$$

The width h is known from the work of Ortwerth and Shine (Reference 4) and others:

$$h = \frac{\pi \lambda x}{\sigma_o} g(M_1) \tag{6}$$

where function $g(M_1)$ contains the "thickening" effect caused by the Mach number, and σ_o is the incompressible spreading parameter to be discussed farther below.

In this work it was necessary to express $g(M_1)$ analytically so that transition calculations might be done. Calculated values are available from Ortwerth and Shine (Reference 4) and Oh (Reference 5) as well as experimental data from a number of sources (see Reference 5). The differences among these values of $g(M_1)$ are not significant, however, and it was decided to compromise by curve-fitting $g(M_1)$ into:

$$g(M_1) = 0.3 + 0.7 \exp(-0.064 M_1^4) \tag{7}$$

1.2.2.3 Fluctuation Intensity

According to Ortwerth, the dividing-streamline fluctuation intensity is:

$$u' = 0.16 \Gamma(M_1)(u_1 - u_2) = 0.16 \Gamma(M_1) \frac{2\lambda}{\lambda + 1} u_1 \tag{8}$$

Like the function $g(M_1)$, $\Gamma(M_1)$ was for convenience approximated by:

$$\Gamma(M_1) = \exp(-0.42 M_1) \tag{9}$$

1.2.2.4 The Turbulence Reynolds Number

If we combine the above equations into Equation (1) we obtain:

$$Re_\Lambda(x) = \left(\frac{u_1 x}{\upsilon_1}\right)\left[0.32\, c_1 \frac{\pi}{\sigma_o}\right] \Gamma(M_1)\, g(M_1) \left(\frac{T_1}{T}\right)^{\frac{k+1}{2}} \frac{\lambda^2}{\lambda + 1} \tag{10}$$

The critical value Re_{Λ_o} can be used to form a constant

$$C = \frac{Re_{\Lambda_o}}{0.32\, c_1 \frac{\pi}{\sigma_o}} \tag{11}$$

Then the transition Reynolds number is, from (10):

$$Re_{XT} = \frac{C}{\Gamma(M_1)g(M_1)} \left(\frac{T}{T_1}\right)^{k+1} \frac{\lambda + 1}{\lambda^2} \qquad (12)$$

with

$$Re_{XT} = \frac{u_1 X_T}{\upsilon_1} \qquad (13)$$

X_T = transition distance from flow origins.

This is the desired end product for the transition distance. It depends on λ not only by the factors shown on Equation (12), but also implicitly through the ratio T/T_1 (see Equation (4)). The same temperature ratio also includes the dependence on T_{02}/T_{01}, via Equation (4), as well as the implicit dependence on M_1 additional to the factor $\Gamma(M_1)g(M_1)$ in Equation (12).

The relation (12) is plotted on Figures 1 and 2. In these graphs we plot Re_{XT}/C in order to delay discussion of the constant C and to allow the latter to adjust itself to future improvements of the numerical constants composing it. The plots show clearly the downstream movement of the transition point (tone) as M_1 increases and as λ decreases. Qualitatively this behavior is not unexpected and agrees with earlier and current popular notions of FSL transition; quantitatively, however, there are substantial differences, as will be discussed below, for example in the dependence of transition on λ.

1.2.3 EVALUATION OF THE NUMERICAL CONSTANTS

Accurate knowledge of the constituents of the constant C of Equation (11) are needed for numerical application of the transition prediction (Equation (12)). In previous work (see Discussion in Reference 1) the threshold turbulence Reynolds number $Re_{\Lambda o}$ had been found to be approximately 15. Use of the same value in Equation (11) is highly desirable because it will test, in the long run, the general validity of the present approach to the transition problem.

No information seems to exist for shear layers on the constant c_1 relating the integral scale and the layer width (in Equation (5)). In fact, what is needed is the value or variation of c_1 as a function of M_1, λ, T_{02}/T_{01}, etc. including its change, if any, across the layer. This serious shortcoming will be met here by assuming $c_1 = 0.2$, a value deriving from wake (Reference 6) and boundary layer studies (Reference 1).

The factor 0.32 in Equation (11) derives from the magnitude, measured by several workers, of u' at its maximum point in the shear layer (the usual

finding is 0.16 $(u_1 - u_2)$, and here a factor of 2 is added by the algebraic sequence of events). There is no information assuring us that this value is unaffected by heat transfer ($T_{02}/T_{01} \neq 1$). Actually, experimental data on u' are very scarce for $M_1 > 0$, as well as for sufficient number of λ values; this issue is certainly far from settled.

Using the most commonly known values of c_1, Re_{Λ_o}, etc. (the spreading parameter $\sigma_o = 11.3$) we can then compute:

$$C = \frac{Re_{\Lambda_o} \sigma_o}{0.32 \pi c_1} = \frac{15 \times 11.3}{0.32 \times 3.14 \times 0.2} \simeq 843 \qquad (14)$$

1.24 DISCUSSION OF THE TRANSITION EQUATION

Equation (12) as demonstrated in Figures 1 and 2, and augmented by the value of C given above, presents as complete a set of predictions as ever attempted up to the present. The increase of Re_{XT} with decreasing λ is precipitous; the physics of the problem, of course, support this finding: at $\lambda = 0$, the Re_{XT} should be infinite on physical arguments alone. When $\lambda = 1$ (i.e. $u_2 = 0$) on the other hand, values of Re_{XT} as low as 2C ($\simeq$ 1700) are obtained in the common case of incompressible, adiabatic flow of air (Figure 1). This value has already increased to 100C by the time λ has decreased to 0.1 ($u_2 = 0.82u_1$).

The increase in Re_{XT} is also very fast with M_1. If we think of the case $u_2 = 0$ ($\lambda = 1$) Re_{XT} increases by a factor of 500 between $M_1 = 0$ and $M_1 = 5$ in the adiabatic case. It should be stressed that this is the first formal enunciation of a formula on FSL transition giving quantitatively the Mach number (compressibility) dependence.

This is also the first occasion in which the transition distance is shown to depend quantitatively on heat transfer, through T_{02}/T_{01}. The typical computation of Figure 2 is done for three values of T_{02}/T_{01}. Shown is the result that as the stream adjacent to the "fast" (subscript "1") stream is heated, the FSL transition point or zone moves aft; however, the dependence of X_T on T_{02}/T_{01} is not apparently as strong as the dependence on M_1 and λ. A noteworthy feature is the variation of Re_{XT} with λ when $T_{02}/T_{01} = 1/3$. Here it seems that for certain M_1 values the transition zone becomes insensitive to λ. Computations at even smaller values of T_{02}/T_{01} would be worthwhile in this context.

There is very little previous theoretical work for comparison with Equation (12). Until recently it was thought that the parameter $Re_{XT}\lambda$ depended only on M_1, i.e. that

$$Re_{XT} \sim \frac{1}{\lambda}$$

Equation (12) shows that the dependence of Re_{XT} on λ is much more complex algebraically; as Figure 2 shows, its curves have a slope varying from 0 to $1/\lambda^2$ depending on M_1 and λ, as well as on T_{02}/T_{01}.

In the proposal phase of this work (Reference 8), this author had used a slightly modified version of the present approach to derive a transition formula for incompressible, adiabatic shear layers:

$$Re_{XT} = c' \frac{\lambda + 1}{\lambda^2}, \quad c' \text{ is a constant} \tag{15}$$

Indeed, for $T_{02}/T_{01} = 1$, $M_1 = 0$, Equation (12) reads

$$Re_{XT} = C \frac{\lambda + 1}{\lambda^2} \tag{16}$$

with C as described by Equation (11). In the same document, the author had attempted a guess at the extension of (15) for compressible flows, using the then-available test data of Birch and Keyes (Reference 3) and of Crawford (Reference 9),:

$$Re_{XT} = \frac{\exp (1.52M_1 + 6.9)}{\lambda} \tag{17}$$

This expression is, thus, essentially the locus of the earlier FSL transition data and is plotted on Figure 3 in comparison with the present theory. The agreement is surprisingly good and acts as a strong endorsement of Equation (12), as well as it assures that the constant C and its ingredients (see Section 1.2.3) are numerically close to the figures quoted.

Ortwerth (Reference 4) has advanced computations of Re_{XT} which follow the spirit of Equation (12). His major criterion for transition is closely related to the critical values of Re_{Λ_θ} advanced herein (Reference 8) and his numerical estimates of Re_{XT} appear close to those given by Equation (12).

A comparison of Equation (12) with the data obtained in the present experiment will be given in Section 1.5.7.

1.2.5 QUALIFICATION TO THE THEORY

As the reader is well aware, the theory outlined above circumvents several conceptual, as well as quantitative issues. A partial list of these conceptual "short cuts" is as follows:

(a) Transition is supposed to occur at a point; actually, it occurs over a finite region which may be quite long.

(b) In measuring X_T, the virtual origin of the flow is not discussed. Generally the virtual origin is not known "a priori" for any given flow.

(c) Transition is supposed to occur when the Re_Λ on the dividing streamline (or the maximum Re_Λ at any flow section) reaches the critical value Re_{Λ_0}. This is equivalent to saying that a FSL can be called turbulent even if turbulence is confined only to an infinitensimally thin layer along the dividing streamline, a clearly unacceptable concept. The application of the present theory to the boundary-layer (Reference 2) discloses that the consideration of the off-axis turbulence is both necessary and tedious.

(d) It is assumed that a fully-developed FSL occurs immediately after transition. Actually, a non-equilibrium region should exist between the transition tone and the attainment of self-preservation.

(e) The theory does not provide for a dependence of X_T on Re', contrary to the existing observations.

(f) The theory disregards initial momentum defects, treating the slipstream trailing a shock intersection in the same way as two boundary layers merging downstream of a partition.

As noticed, the theory also utilizes information drawn from the turbulent state of the FSL; yet this information is woefully inadequate because of the lack of suitable measurements. Examples are:

(g) The theory utilizes, essentially, Ortwerth's theory (Reference 4) on the variation of the (maximum) u', which is in turn verified only by very limited data. For example, $u'(M_1)$ is known only at one supersonic Mach number (Reference 10). There is not information on the dependence of u' on T_{02}/T_{01} or on λ at supersonic speeds.

(h) The integral scale Λ is assumed to be h/5 only by inference from wake and boundary layer data. There are no appropriate measurements of Λ.

(i) The kinematic viscosity is seemingly secured by the use of the linear Crocco relation. Yet, both in boundary layers (Reference 11) and wakes (Reference 12) the linear Crocco relation is now known to represent a singularity for Prandtl number equal to unity only, while it may vary considerably for, say $T_{02}/T_{01} \neq 1$.

The preceding list should convince the reader that additional work is needed, not only to improve Equation (12), but also to produce the experimental data on which that formula depends. Recommendations to this effect are made in Section 1.7.

1.3 EXPERIMENT OBJECTIVE AND DESIGN

The objective of the experimental work was to generate a free shear layer from which transition data could be obtained, for comparison with the theory of Section 1.2. The method of generating the FSL became an important issue at the outset of this work. In practice, most FSL's of interest are those between two co-flowing streams, e.g. a nozzle discharging a stream parallel to, and into, an external stream. This method was shunned, however, because of the interfering effect of the boundary-layer growing on the partition separating the two streams. It was therefore decided to generate a "pure" FSL by utilizing the slipstream emanating from the intersection of two oblique shockwaves in supersonic flow, a method previously used also by Birch and Keyes (Reference 3). In contrast to the experiment done by the latter, it was decided to utilize two planar shocks in order to avoid pressure gradient effects generated when one or both of the shock waves is curved.

Considerable work went into the design of the method for intersecting two shock waves. One of the alternatives studied, for example, was two opposing wedges resembling a supersonic diffuser inlet; this was rejected in the end because the "strength" of the slipstream produced with it (i.e. the difference of flow speed across the FSL) could not be raised without choking the diffuser inlet. The design finally chosen consisted of two shock waves of the same family generated by a double wedge, i.e. a sharp-lipped flat plate with a wedge indentation parallel to and downstream from, the leading edge. The flow produced by this arrangement is shown on Figure 4. Computations were made to see what strength of FSL could be produced as a function of the free stream Mach number M_∞ and the angles α_1 and α_2. It was found that if $M_\infty < 6$ or so, the FSL strength was negligible for all practical angles α_1 and α_2. For M_∞ in excess of 8, on the other hand, the FSL strength did not increase much beyond what could be attained at $M_\infty = 8$. Since the latter M_∞ was also the design Mach number of AEDC Tunnel B, it was chosen to be the stream Mach number.

Figure 5 shows the FSL strength attainable at Mach 8, expressed in terms of the velocity difference:

$$1 - \frac{u_2}{u_1}, \text{ and } \lambda = \frac{u_1 - u_2}{u_1 + u_2}$$

as a function of α_1 and α_2. Since shock separation lies beyond the bounds of the plot, it appears that the desired operation would occur around, say, $\alpha_1 = 20^\circ$ and $\alpha_2 = 20^\circ$. However, wind-tunnel choking is a problem when the

frontal area of the model placed in Tunnel B exceeds about 200 $in.^2$ for the available indented-plate model (see Section 1.4.2). Furthermore, boundary-layer separation could occur if α_2 was large; in Figure 5 the chosen α_1 and α_2 should stay to the left of the dotted lines which represent estimates of maximum allowable α_2 before separation occurs. For a laminar boundary layer on the base plate (Figure 4) we see that Hankey's criterion (Reference 13) precludes all but the smallest α_1 and α_2 angles. For turbulent separation, on the other hand, Reeve's criterion (Reference 14) implies attached flow for all but the largest α_2 angles. This criterion and the "frontal area" curve marked "200 $in.^2$" enclose the area in which the choices of α_1 and α_2 are restricted.

The conditions finally chosen are shown as calculated on the following Table I. Subscript 1, as per the usual FSL convention of marking the "fast" and "slow" side, represents the fast side which, according to Figure 4, lies closest to the plate. According to this Table, if the indented plate model was configured according to the last two lines of the Table at $M_\infty = 8$, the other conditions would be obtained, regardless of the P_o and T_o of the wind-tunnel. However, estimates for each condition shown were made with Equation (17), to ensure that the available P_o range would cause transition (for each condition) to appear within a few inches from the origin of the FSL (i.e. the oblique shock intersection). This was important in order to utilize the main diagnostic tool, which was the tunnel shadow graph system.

The experiment design also sought to guarantee the attainment of the conditions of Table I by insuring two-dimensional flow, which was the basis of all computations made. Specifically, it was attempted to make the model as wide as possible in order to avoid edge effects. The desired width was the main reason for making the model large and introducing the wind-tunnel blockage (choking) considerations referred to earlier. A flat plate model of the proper width was actually available at AEDC, so that model fabrication at Aeronutronic was limited to modifications needed to add a ramp (or "wedge plate") to this model.

The experiment design was implemented at AEDC, which provided the wind-tunnel and test support services. The description of the test hardware which follows is drawn primarily from AEDC Report TSR-79-V30 (Reference 15).

1.4 EXPERIMENTAL EQUIPMENT

1.4.1 TEST FACILITY

VKF Wind Tunnel B is a closed-circuit hypersonic wind tunnel with a 50-in. diam. test section. Two axisymmetric contoured nozzles are available to provide Mach numbers of 6 and 8 and the tunnel may be operated continuously over a range of pressure levels from 20 to 300 psia at Mach number 6, and 50 to 900 psia at Mach number 8, with air supplied by the VKF main compressor plant. Stagnation temperatures sufficient to avoid

TABLE I

THREE OPERATING CONDITIONS SELECTED FOR THE TEST

Condition	1	2	3
M_1	3.52	3.92	3.28
M_2	2.34	3.01	2.43
u_2/u_1	0.857	0.924	0.891
λ	0.077	0.039	0.058
ρ_2/ρ_1	0.604	0.691	0.691
α_1 (deg)	15	15	20
α_2 (deg)	15	10	10

air liquefaction in the test section (up to 1350°R) are obtained through the use of a natural gas fired combustion heater. The entire tunnel (throat, nozzle, test section, and diffuser) is cooled by integral, external water jackets. The tunnel is equipped with a model injection system, which allows removal of the model from the test section while the tunnel remains in operation. A description of the tunnel may be found in Reference 16. In this experiment the tunnel was operated at Mach 8.

1.4.2 MODEL

This model, illustrated in Figure 6, consisted of a 20-in.-wide sharp flat plate with a ramp attachment positioned 8.5 in. from the leading edge. Brackets located between the ramp attachment and the flat plate were bolted together to set and maintain the ramp inclination at 10-, 15-, or 20-deg with respect to the flat plate, using a predetermined bolt hole pattern. The underside of the ramp leading edge was bevelled to mate to the flat plate surface when the inclination angle of the ramp was 10 degrees. Spacers were provided to support the ramp leading edge for inclination angles of 15- and 20-deg. No seal was used between the ramp leading edge and the flat plate.

To minimize flow separation in the compression corner, it was desirable to maintain a turbulent boundary layer ahead of the flat plate-ramp junction. For this purpose, distributed roughness elements (No. -40 grit) was used as a boundary-layer tripped mechanism. Particles were applied in a 1.5 in.-wide band parallel to and 0.5 in. aft of the leading edge of the flat plate.

Twenty-four pressure orifices were used to measure model surface pressures and monitor any lateral pressure gradients existing on the surface. The locations of the orifices are indicated in Figure 6.

The ramp was designed and fabricated by FACC to be fitted to an existing VKF flat plate model.

1.4.3 INSTRUMENTATION

Three types of diagnostic instrumentation were used:

(a) Pitot tube, for flow field measurements and transition detection.

(b) Shadowgraph system for transition detection.

(c) Model surface static pressures for flow field measurements.

Surveys of the free shear layer were made using a retractable overhead probe drive system (X-Z Survey Mechanism) designed and fabricated by the VKF. The mechanism is housed in an air lock located immediately above a port in the top of the Tunnel B test section. Access to the test section is through a 40-in.-long, 4-in.-wide opening which can be sealed by a

pneumatically-operated door when the mechanism is retracted. Separate drive motors are provided to (1) insert the mechanism into the test section or retract it into the housing, (2) position the mechanism at any desired axial station over a range of 35 in. with an uncertainty of $\pm$0.01 in., and (3) survey a flow field of approximately 10-in. depth with an uncertainty of $\pm$0.001 in.

For the present test an additional drive mechanism was attached to the foot of the vertical-drive (flow field survey) strut (see Figure 7). This unit was a rotary actuator with the probe mounted on a wheel driven by a worm-gear which could sweep the probe tip through a 0.5-in.-length arc of 5-in. radius. The readout potentiometer of the rotary actuator was calibrated for the full-scale travel (arc length) of 0.5-in. and was equipped with a clutch which disengaged the poteniometer drive shaft at either end of the travel. The clutch permitted the probe to be positioned at any desired initial location without affecting the resolution of the readout. The actuator housing afforded storage space to protect probes when not in use. The temperature of the rotary actuator motor was monitored throughout the test to insure that an acceptable operating environment was maintained.

To survey the relatively thin shear layer a pitot pressure probe of small dimensions was required to avoid size effects on the resolution of the profiles. The probe was constructed using 32 mil OD and 22 mil ID tubing bent to facilitate alignment with the local flow direction (see Figure 8). The probe was flattened at the tip to further reduce the probe dimension in the plane of survey. The resulting lateral dimension increase was acceptable since the flow field was two-dimensional. The probe was fabricated by the VKF.

Shadowgrams of the flow were obtained using the Tunnel B standard optical system operating both in the spark (short exposure) and continuous (time exposure) modes. The static pressures on the plate surface were measured at the locations indicated on Figure 6.

1.4.4 TE MATRIX AND TEST PROCEDURES

The text matrix shown on Table II indicates that the experiment design points of Table I were fulfilled. The test was conducted with the model placed in the position indicated on Figure 9. Changes in the angle of attack (i.e. the angle α_1, of Table I) we accomplished remotely while the tunnel was running; to change α_2 (the "ramp" or "wedge" angle) the model was withdrawn from the flow, to enable test personnel to work on the model.

Test data in the form of shadowgraphs, model surface pressure measurements, and pitot pressure surveys were obtained for various tunnel conditions. A range of free-stream unit Reynolds numbers of from 0.08- to 0.3-million per in. was covered by varying tunnel pressure P_o between 200 and 800 psia while maintaining a nominally constant tunnel temperature of

T_o = 1320°R. Increments of tunnel pressure of 50 psi were used in acquiring the shadowgraphs and model pressure data and increments of 100 psi for the survey data.

Shadowgraphs of the shear layer were obtained for each test condition. Standard 70-mm film magazine exposures and 4- by 5-in. fast-developing exposures were made. The former provided a file of the shadowgraphs and the latter facilitated rapid examination of the optical data as an aid in directing the course of the investigation. The file of spark-shadowgraph exposures was supplemented for certain test conditions by time exposures made using the continuous light source of the optical system.

Model surface pressure measurements were made along and off centerline for each test condition to assess the plate finite-span effects. The ramp surface (centerline) pressure was also used to supplement the pitot pressure measurements obtained from the surveys of the shear layer.

Pitot pressure profiles of the shear layer were obtained above the ramp near the trailing edge at S = 20 in., approximately. Each survey was begun with the probe immediately below the shear layer, as determined by viewing the images on the shadowgraph screen of the optical system, and the initial length of the pitot probe (see Figure 8) was aligned parallel to the estimated centerline of the shear layer. Measurements of pitot pressure were made at 25 to 35 positions in the shear layer as the probe was driven in discrete steps away from the model. The locus of the probe driven by the rotary actuator was an arc of 5-in. radius and the angle between the radius and the centerline of the shear layer was typically 40 deg. The readout of probe position was limited to a travel of 0.5 in. An arc of 0.5-in. length with a radius of 5.0 is approximately equal to its chord, but the inclination of the chord with respect to the normal to the shear layer resulted in a limitation of probe travel, with readout, to approximately 0.4 in. in the normal direction. For certain test conditions the "thickness" of the shear layer at the survey station was somewhat greater than 0.4 in.; however, this restriction on the available readout of probe position was not considered to be a compromise of the test objective.

It should be noted that the roughness elements used to promote boundary layer transition on the flat plate were progressively eroded from the surface during the testing; however, the shadowgraph pictures of the flow field do not indicate any resulting separation of the boundary layer at the compression corner.

1.5 RESULTS

1.5.1 FLOW FIELD MEASUREMENTS

The flow field achieved for each configuration was important to analyze first, because it shows to what extent the design flows of Table I were achieved.

TABLE II. TEST MATRIX

GROUP	RAMP ANGLE (DEG)	ALPHA (DEG)	M(INF)	PO (PSIA)	TO (°R)	RE(INF) $\times 10^{-5}$ PER IN.	DATA TYPE
1	10	-15.0	7.98	397.6	1333	1.47	Model
2				400.8	1318	1.51	Pressure
3				399.4	1319	1.50	
4				449.7	1322	1.69	
5				500.4	1320	1.88	
6				551.3	1323	2.06	
7			7.99	599.0	1329	2.22	
8				653.0	1318	2.45	
9			7.98	398.0	1323	1.49	
10				352.6	1327	1.31	
11			7.96	298.8	1322	1.13	
12			7.95	252.8	1318	0.962	
13			7.94	204.1	1318	0.779	
14			8.00	699.5	1327	2.59	
15				752.3	1313	2.83	
16				801.8	1310	3.03	
17		-18.0		800.1	1322	2.98	
18		-20.0		802.4	1326	2.97	
19				747.5	1325	2.77	
20				697.4	1325	2.59	
21			7.99	666.9	1325	2.48	
22				653.5	1322	2.44	
23				599.6	1312	2.25	
24				548.7	1324	2.05	
25			7.97	498.1	1328	1.86	
26				446.0	1322	1.68	
27				396.3	1313	1.51	
28		-15.0		399.2	1326	1.49	Model
29				401.2	1316	1.52	Pressure
30			7.94	197.2	1314	0.756	+
31			7.96	304.5	1331	1.14	Flowfield
32			7.97	499.4	1312	1.90	Survey
33			7.99	603.8	1313	2.28	
34*				601.6	1320	2.25	
35				600.5	1312	2.27	
36			8.00	703.2	1317	2.63	
37	15	-15.1	7.97	401.1	1321	1.51	Model
38				350.3	1320	1.32	Pressure
39		-15.0		303.2	1321	1.14	
40			7.95	247.3	1325	0.933	
41			7.97	449.9	1329	1.68	
42				501.6	1311	1.91	
43			7.98	551.8	1316	2.08	
44			7.99	603.2	1325	2.25	
45				649.3	1320	2.43	
46			8.00	701.4	1324	2.61	
47				752.5	1321	2.80	
48				801.9	1321	2.99	
49	10	-20.0	7.97	401.1	1323	1.51	Model
50				501.2	1323	1.88	Pressure
51			7.99	601.2	1317	2.26	+
52		-19.9	8.00	703.1	1330	2.59	Flowfield
53*				804.2	1323	2.99	Survey
54*				801.3	1322	2.98	
55				801.1	1323	2.98	

* Incomplete Survey

Typical plate surface pressure measurements are shown on Table III and Figure 10. Small anomalies in the pressure distribution are insignificant and thought to be caused by operational (e.g. calibration) errors in the data acquisition system. It is seen that the three pressures measured along the span of the wedge plate are very nearly equal, indicating little or no three-dimensionality (edge effects) in that flow.

The measured surface pressures are for the three test configurations have been compared with theory. Generally, the base plate pressures were found about 10% higher than expected, while on the wedge plate they lay below the expected levels by an equal amount. These differences, thought to be due to errors in the angle of attack setting, are at first glance appreciable; but when the angle-of-attack errors needed to produce these differences are computed, the results are much better. It is estimated that these disparities can be caused by misalignments of order 0.01 degree, i.e. less than one minute of arc, which is certainly within the error band of the Tunnel B mechanism at AEDC. It is concluded that the observed surface pressures meet expectations to a high accuracy.

The pitot pressure surveys across the FSL combined with the known tunnel supply pressure and the static pressure (which is, for every data group, identical throughout with the measured wedge or ramp surface pressure) makes it possible to compute the conditions in the two streams (regions 1 and 2 of Figure 4) bounding the FSL. Such conditions include the Mach numbers M_1 and M_2, velocity ratio u_2/u_1 etc., and are typically shown in Table IV, as well as in Figure 11. In the latter it is seen that the design Mach numbers M_1 and M_2 are best attained at the lower tunnel pressure, but all differences are anyway so small that one can safely claim that the design conditions were met. Specifically, Table IV states that the Mach numbers computed by the theory (in the design stage) were duplicated within 1%-2%, the velocity and density ratios within 0.1%-0.3%, and the parameter λ within 2.5%.

It will be noticed that Table IV does not include the case $\alpha_1 = 15^\circ$, $\alpha_2 = 15^\circ$ (Condition 1 of Table I). The flowfield (and the transition) data for this configuration, represented by groups 37 through 48 in the test matrix (Table II) were anomalous and scattered. This problem was explained after the test by the shadowgrams, which showed that the FSL produced by this pair of α_1, α_2 merged and therefore interacted with the boundary layer on the wedge plate. This condition was beyond the scope of this work, and therefore no further analysis of the $\alpha_1 = 15^\circ$, $\alpha_2 = 15^\circ$ case was made.

The discussion has so far dealt with the experimental verification of the edge (boundary) conditions of the FSL; of course, these conditions are very important in the FSL transition data, to be presented below. The flow inside the FSL is equally important, since any anomalies in it would cast suspicion on the quality of the flow and of the experiment itself. Good flow quality has been assured, as was seen by inspection of the documented data. These are given in great detail in the Data Package appended to

TABLE III. FLOW FIELD PROPERTIES, GROUP 35

AEDC (ARO,INC.) ARNOLD AFS, TENNESSEE
VON KARMAN GAS DYNAMICS FACILITY 50 INCH HYPERSONIC TUNNEL B
SAMSO/AFOSR/FORD AEROSPACE AND COMMUNICATIONS CORPORATION SHEAR LAYER TEST
V418-42

DATA TYPE 4
FLOW FIELD SURVEY
PROBE EXT

CONFIGURATION 1

SMOOTH WALL CONFIGURATION

LOOP	PO (PSIA)	TO (DEG R)	PP(INF) (PSIA)	P(INF) (PSIA)	H(P) (IN)	PP (PSIA)	PW (PSIA)
1	600.47	1311.7	5.125	0.062	0.0000	26.321	1.377
2	601.27	1311.7	5.132	0.062	0.0115	26.412	1.377
3	601.17	1311.7	5.131	0.062	0.0233	26.281	1.378
4	600.27	1311.7	5.124	0.062	0.0342	26.130	1.377
5	600.27	1311.7	5.124	0.062	0.0454	25.918	1.377
6	600.37	1311.7	5.125	0.062	0.0577	25.626	1.377
7	600.67	1311.7	5.127	0.062	0.0691	25.183	1.376
8	600.77	1311.7	5.128	0.062	0.0807	24.669	1.377
9	600.07	1311.7	5.122	0.062	0.0934	23.954	1.377
10	600.37	1311.7	5.125	0.062	0.1046	23.189	1.376
11	600.77	1311.7	5.129	0.062	0.1166	22.322	1.377
12	600.17	1312.7	5.123	0.062	0.1268	21.537	1.376
13	600.67	1312.7	5.127	0.062	0.1392	20.650	1.377
14	600.87	1312.7	5.129	0.062	0.1510	19.875	1.376
15	600.37	1312.7	5.125	0.062	0.1619	19.140	1.376
16	600.27	1312.7	5.124	0.062	0.1745	18.283	1.377
17	600.57	1313.7	5.126	0.062	0.1854	17.709	1.377
18	600.67	1313.7	5.127	0.062	0.1971	17.135	1.378
19	601.17	1313.7	5.131	0.062	0.2086	16.702	1.378
20	600.77	1313.7	5.128	0.062	0.2225	16.330	1.378
21	599.97	1313.7	5.121	0.062	0.2314	16.158	1.377
22	600.97	1314.7	5.130	0.062	0.2434	16.017	1.376
23	600.87	1314.7	5.129	0.062	0.2549	15.917	1.377
24	601.17	1314.7	5.131	0.062	0.2669	15.836	1.376
25	600.97	1314.7	5.130	0.062	0.2785	15.816	1.378
26	601.37	1314.7	5.133	0.062	0.2912	15.786	1.377
27	600.37	1314.7	5.125	0.062	0.3022	15.796	1.377
28	600.97	1314.7	5.130	0.062	0.3127	15.776	1.377
29	601.17	1315.7	5.131	0.062	0.3248	15.816	1.379
30	600.57	1315.7	5.126	0.062	0.3361	15.846	1.377
31	600.97	1315.7	5.130	0.062	0.3476	15.876	1.378
32	600.87	1315.7	5.129	0.062	0.3596	15.917	1.378
33	600.77	1316.7	5.128	0.062	0.3708	15.967	1.377
34	601.37	1316.7	5.133	0.062	0.3708	15.977	1.379

MEAN VALUES

ROLL =	0.1 DEG	PO =	600.7 PSIA	P(INF) =	0.0620 PSIA
M(INF) =	7.99	TO =	1313.5 DEG R	PW =	1.377 PSIA
ALPHA =	-15.03 DEG	PP,(INF) =	5.128 PSIA		
		RE(INF) =	2.265E+05 PER IN	U(INF) =	3825.8 FT/SEC
		MU(INF) =	7.677E-08 LBF-SEC/FT2	Q(INF) =	2.772 PSIA
		RHO(INF) =	1.755E-03 LBM/FT3	T(INF) =	95.4 DEG R

TABLE III. (CONT'D)

AEDC (ARO,INC.) ARNOLD AFS, TENNESSEE
VON KARMAN GAS DYNAMICS FACILITY 50 INCH HYPERSONIC TUNNEL B
SAMSO/AFOSR/FORD AEROSPACE AND COMMUNICATIONS CORPORATION SHEAR LAYER TEST
V41B-42

DATA TYPE 4
FLOW FIELD SURVEY
PROBE EXT

CONFIGURATION 1
SMOOTH WALL CONFIGURATION

LOOP	M(P) (IN)	PP/PPE	M(P)	M(P)/ME	TT (DEG R)	TT/TTE	T (DEG R)	U (FT/SEC)	U/UE	RE/IN	RET/IN
1	0.0000	1.647	3.80E+00	1.295	1311.7	0.996	336.7	3.423E+03	1.081	3.736E+05	1.371E+05
2	0.0115	1.653	3.81E+00	1.297	1311.7	0.996	335.8	3.424E+03	1.082	3.756E+05	1.375E+05
3	0.0233	1.645	3.80E+00	1.294	1311.7	0.996	337.2	3.422E+03	1.081	3.726E+05	1.369E+05
4	0.0342	1.635	3.79E+00	1.290	1311.7	0.996	338.5	3.420E+03	1.080	3.695E+05	1.362E+05
5	0.0454	1.622	3.78E+00	1.285	1311.7	0.996	340.6	3.416E+03	1.079	3.648E+05	1.352E+05
6	0.0577	1.604	3.75E+00	1.279	1311.7	0.996	343.5	3.411E+03	1.078	3.585E+05	1.338E+05
7	0.0691	1.576	3.72E+00	1.267	1311.7	0.996	348.0	3.403E+03	1.075	3.490E+05	1.318E+05
8	0.0807	1.544	3.68E+00	1.253	1311.7	0.996	353.6	3.393E+03	1.072	3.380E+05	1.294E+05
9	0.0934	1.499	3.63E+00	1.234	1311.7	0.996	361.4	3.379E+03	1.068	3.232E+05	1.260E+05
10	0.1046	1.451	3.57E+00	1.214	1311.7	0.996	370.1	3.364E+03	1.063	3.077E+05	1.225E+05
11	0.1166	1.397	3.50E+00	1.190	1311.7	0.996	380.7	3.345E+03	1.057	2.905E+05	1.184E+05
12	0.1268	1.348	3.43E+00	1.169	1312.7	0.997	390.9	3.328E+03	1.051	2.752E+05	1.147E+05
13	0.1392	1.293	3.36E+00	1.143	1312.7	0.997	403.1	3.306E+03	1.044	2.586E+05	1.105E+05
14	0.1510	1.244	3.29E+00	1.121	1312.7	0.997	413.9	3.286E+03	1.038	2.446E+05	1.069E+05
15	0.1619	1.198	3.23E+00	1.099	1312.7	0.997	425.2	3.266E+03	1.032	2.316E+05	1.034E+05
16	0.1745	1.144	3.15E+00	1.073	1312.7	0.997	439.2	3.240E+03	1.024	2.168E+05	9.947E+04
17	0.1854	1.108	3.10E+00	1.056	1313.7	0.998	449.3	3.223E+03	1.018	2.070E+05	9.664E+04
18	0.1971	1.072	3.05E+00	1.037	1313.7	0.998	459.6	3.203E+03	1.012	1.976E+05	9.394E+04
19	0.2086	1.045	3.01E+00	1.024	1313.7	0.998	467.6	3.189E+03	1.007	1.906E+05	9.190E+04
20	0.2225	1.022	2.97E+00	1.012	1313.7	0.998	474.7	3.175E+03	1.003	1.848E+05	9.015E+04
21	0.2314	1.011	2.96E+00	1.006	1313.7	0.998	477.9	3.169E+03	1.001	1.821E+05	8.933E+04
22	0.2434	1.003	2.94E+00	1.002	1314.7	0.998	480.8	3.165E+03	1.000	1.798E+05	8.85RE+04
23	0.2549	0.996	2.93E+00	0.999	1314.7	0.998	482.9	3.161E+03	0.999	1.782F+05	8.811E+04
24	0.2669	0.991	2.93E+00	0.996	1314.7	0.998	484.4	3.159F+03	0.998	1.770E+05	8.772E+04
25	0.2795	0.990	2.92E+00	0.995	1314.7	0.998	485.3	3.157E+03	0.997	1.766F+05	8.765F+04
26	0.2912	0.988	2.92E+00	0.994	1314.7	0.998	485.6	3.156E+03	0.997	1.762E+05	8.749E+04
27	0.3022	0.989	2.92E+00	0.995	1314.7	0.998	485.5	3.156E+03	0.997	1.763E+05	8.755E+04
28	0.3127	0.987	2.92E+00	0.994	1314.7	0.998	485.9	3.156E+03	0.997	1.760E+05	8.745E+04
29	0.3248	0.990	2.92E+00	0.995	1315.7	0.999	485.8	3.158E+03	0.998	1.764F+05	8.758E+04
30	0.3361	0.992	2.93E+00	0.996	1315.7	0.999	484.9	3.160E+03	0.998	1.769E+05	8.771E+04
31	0.3476	0.994	2.93E+00	0.997	1315.7	0.999	484.4	3.160E+03	0.998	1.774E+05	8.786E+04
32	0.3596	0.996	2.93E+00	0.998	1315.7	0.999	483.6	3.162E+03	0.999	1.780E+05	8.805E+04
33	0.3708	0.999	2.94E+00	1.000	1316.7	1.000	482.7	3.166E+03	1.000	1.787E+05	8.820E+04
34	0.3708	1.000	2.94E+00	1.000	1316.7	1.000	482.9	3.165E+03	1.000	1.787E+05	8.826E+04

MEAN VALUES

POLL = 0.1 DEG PO = 600.7 PSIA PPE = 1.598E+01 PSIA
M(INF) = 7.99 TO = 1313.5 DEG R PW = 1.377 PSIA ME = 2.938E+00
ALPHA = -15.0 DEG P(INF) = 0.0620 PSIA TTE = 1.317E+03 DEG R
T(INF) = 95.4 DEG R PE(INF) = 2.265E+05 PER IN UE = 3.165E+03 FT/SEC

TABLE III. (CONCLUDED)

AEDC (ARO,INC.) ARNOLD AFS, TENNESSEE
VON KARMAN GAS DYNAMICS FACILITY 50 INCH HYPERSONIC TUNNEL B
SAMSO/AFOSR/FORD AEROSPACE AND COMMUNICATIONS CORPORATION SHEAR LAYER TEST
V41B-42

CONFIGURATION 1

SMOOTH WALL CONFIGURATION

DATA TYPE 4
FLOW FIELD SURVEY
PROBE EXT

MODEL SURFACE MEASUREMENTS

ORFICE NO.	S (IN)	PW (PSIA)	DELTA PW (PSIA)
1	0.530	0.9470	0.0041
2	2.150	0.5943	0.0054
3	2.380	0.6159	0.0023
4	2.630	0.6164	0.0008
7	3.880	0.6588	0.0014
8	4.380	0.6668	0.0011
9	4.880	0.6720	0.0010
10	5.380	0.6617	0.0009
11	5.880	0.6616	0.0005
12	6.880	0.6578	0.0007
13	7.880	0.6521	0.0003
22	16.590	1.3518	0.0007
23	16.590	1.3772	0.0008
24	16.590	1.3464	0.0007

MEAN VALUES

ROLL = 0.1 DEG
M(INF) = 7.99
ALPHA = -15.0 DEG

PO = 600.7 PSIA
TO = 1313.5 DEG R
P(INF) = 0.0620 PSIA
T(INF) = 95.4 DEG R

TORK = 73.0 DEG F
TEXT = 90.0 DEG F

TABLE IV.

RESULTS OF FLOW FIELD SURVEYS

Configuration	2	3
α_1 (DEG)	15	20
α_2 (DEG)	10	10
M_1 (Average)	3.85	3.23
(Theoretical Expectation)	(3.92)	(3.28)
M_2 (Average)	2.95	2.39
(Theoretical Expectation)	(3.01)	(2.43)
U_2/U_1 (Average)	0.922	0.888
(Theoretical Expectation)	(0.924)	(0.891)
λ (Average)	0.0404	0.0591
(Theoretical Expectation)	(0.0395)	(0.0576)
ρ_2/ρ_1 (Average)	0.692	0.689
(Theoretical Expectation)	(0.691)	(0.691)

Reference 15. An example is given here for Group 35, in Table III and Figures 12 through 15. Note that beside the Mach number distribution across the FSL, we plot the ratio M/M_2, u/u_2, T/T_2, etc.

Figure 16 shows an important element of this measurement, which is the verification of the "Crocco" relation across the FSL (see Appendix). The Crocco relation, given in Equation (A.1), features decisively in the transition theory of Section 1.2; if it were invalid, the results of Section 1.2 would be invalid also. Figure 16 shows that the agreement between the data (here represented at random by Groups 35 and 51) and Equation (A.1) is indeed very good.

In summary, the flow field data taken with the pitot probe and the model surface pressures have shown that the desired flow was achieved with high precision for the two configurations 2 and 3 of Table I. This flow can next be used to interpret the transition observations.

1.5.2 TRANSITION TO TURBULENCE

The diagnostic tool for turbulence detection was the shadowgraph system. The principle of detection rests on the fact that laminar shear flows usually have large density gradients which decrease, due to enhanced spreading and diffusion, when the flow becomes turbulent. Since optical systems produce a response proportional to derivatives of the density they can be used for transition detection. On shadowgrams, for example, a laminar flow would appear dark (black), and transition would be indicated in the region where the flow becomes lighter. Quite frequently, too, the eddy structure of the turbulence is directly visible on short-exposure photographs taken with a good schlieren or shadowgraph system. A trained observer can utilize such a system to detect transition faster and more economically than by using other sensors.

Figures 17 and 18 show the flow field as observed by the spark and time-exposure shadowgraph. The flow field follows quite faithfully the theoretical construction of Figure 4 and the zone of transition in the FSL is quite clear. The time exposure, especially, bears out fully the hypothesis that the FSL "disappears" after transition. The transition zone is marked on each picture as determined by visual inspection; note that Figures 17 and 18 do not represent the same conditions. The transition distance X_T is measured from the FSL origin (the crossing of the two original shocks) and the transition point so determined.

ARO, Inc. developed another approach in processing the same photo prints from the shadowgraph system, which consists of scanning the photographs such as shown on Figures 17 and 18, with an optical densitometer. Iso-density contours (here "density" refers to that of the photo print contrast level) can be plotted directly as in Figure 9, page 22, of Reference 15, or broken up into profiles of optical density ("grey level") such as shown on Figure 19. Low grey levels in this figure identify regions

seen as dark or black by the viewer of Figures such as 17 or 18. As expected, the dip, which in Figure 19 represents the FSL, gets deeper (darker) as one approaches the FSL origin. This method is supported by automated equipment at ARO, and thus recommends itself for this transition detection problem.

Only a limited amount of work was done with this technique for this test, mainly as an exploratory evaluation of it for future use. Although based on the same principle as the visual inspection of photographs (the recognition of varying shades of grey), the densitometer method eliminates observer bias by assigning numerical values to these shades. The question therefore is whether the densitometer method agrees with the visual method employed here to measure X_T for each of the conditions listed on Table I. To check this, the densitometer results are compared with the visual results on Figure 20. Transition in the FSL occurs where the densitometer trace departs from "black" toward "white". It is seen that, for this group of data, this occurs exactly where the visual technique also put transition. The visual method is thus supported by the densitometer method.

The transition distance X_T was measured visually for each of the two spark pictures taken at each of the conditions tested (i.e. the data groups of Table II). The X_T's listed on Table V and plotted on Figure 21 show an error band whose two extremities are fixed by the two photographs at each data group; that is, each of the two photos gives, generally, a slightly different X_T. This is to be expected, since for each condition transition usually "jitters", i.e. oscillates randomly about its mean position. However, the transition Reynolds numbers on Table V have been averaged between the two data points for each data Group.

It is immediately seen on Figure 21 that X_T increases (in fact, almost linearly) with P_o. This is surprising, since Section 1.2 indicates a constant Re_{XT} regardless of P_o. Thus, according to Equation (12) the X_T should <u>decrease</u> as P_o increases, an expectation common to all shear flows. Figure 21 says that Re_{XT} increases rapidly with P_o, both because P_o increases and because X_T increases. According to Table V Re_{XT}, far from being constant, varies from 1 to 5 million for $\alpha_1 = 15^o$, $\alpha_2 = 10^o$, ($\lambda = 0.04$) as P_o varies from 200 to 800 psia; Re_{XT} varies from about 2 to 4 million for $\alpha_1 = 20^o$, $\alpha_2 = 10^o$ over the same P_o range.

The unexpected fact that Re_{XT} thus varies with unit Reynolds number is reminiscent of the unit Reynolds number effect on boundary layer transition. In that instance, increasing the wind-tunnel P_o generates increased acoustic boundary-layer radiation from the tunnel sidewall and accelerates transition, spoiling the "constant Re_{XT}" concept. Here, however, the effect is going the "wrong way", since an increase in P_o <u>increases</u> Re_{XT}. The result of Figure 21 cannot be attributed, therefore, to the customary sidewall radiation effect. The series of shadowgrams shown on Figure 22 indicate just how X_T increases as P_o increases.

TABLE V. MEASURED TRANSITION DISTANCES

$\alpha_1 = 15°, \alpha_2 = 10°$

GROUP	X(INCH) FIRST PHOTO	X(INCH) SECOND PHOTO	PO(PSIA)	RE' $(INCH)^{-1}$ $X10^5$	RE_{XT} $X10^5$
4	6.73	6.73	450	2.93	19.7
5	6.73	6.53	500	3.21	21.3
6	7.52	8.31	550	3.49	27.6
7	8.31	8.91	600	3.75	32.3
8	9.3	9.3	650	4.05	37.7
9	6.23	6.43	400	2.65	16.7
10	6.04	5.74	350	2.33	13.7
11	5.15	5.54	300	2.33	13.7
12	4.16	4.45	250	1.7	7.3
13	4.55	4.55	200	1.39	6.26
14	-	9.3	700	4.35	43.5
15	Large	Large	750	4.66	-
16	Large	Large	800	4.97	-
28	6.33	6.33	400	2.65	16.7
30	3.56	3.95	200	1.39	5.3
32	4.35	4.75	500	3.21	17.3

$\alpha_1 = 20°, \alpha_2 = 10°$

17	8.71	Large	800	3.96	37.6
18	7.72	7.92	800	3.96	30.9
19	7.32	7.32	750	3.78	27.6
20	6.93	6.93	700	3.59	24.8
21	7.2	7.2	650	3.36	24.2
22	6.33	6.33	650	3.36	22.2
23	6.53	6.33	600	3.12	20
24	5.14	5.54	550	2.88	15.3
25	5.54	5.14	500	2.63	13.9
26	4.16	4.35	400	2.14	9.2
49	4.75	5.34	400	2.14	10.9
50	5.94	8.2	500	2.63	15.5
51	5.54	6.33	600	3.12	19.3
52	7.32	6.63	700	3.59	25.1
53	7.52	7.32	800	3.92	29

1.5.3 COMPARISON OF THEORY WITH EXPERIMENT

The first concern in examining the present data centers around the unit Reynolds number effect just discussed. To this end, we present Figure 23 which plots the present Re_{XT} measurements as a function of the unit Reynolds number (equivalent to P_o):

$$Re' = \frac{u_1}{\upsilon_1}$$

As already discussed, the data are very sensitive to Re'. Plotted for comparison are also Crawford's data (Reference 9). We see that these measurements, too, show a clear dependence on Re', and that they furthermore increase as Re' increases. This increase is not as pronounced as in the present test, and Crawford actually found that his X_T decreased as Re' increased. Nevertheless Crawford, too, has apparently found an Re' dependence and in the same sense as the present measurements.

The theory of Section 1.2 does not reveal a dependence of Re_{XT} on Re', and hence the issue remains unresolved. It should be noted that any theory in which X_T is cast in terms of Re_{XT} will be similarly impotent in yielding a unit Reynolds number dependence. To avoid speculation, this matter will be left aside and the present data will have to be discussed further as an "error bar" in the Re_{XT}, M, λ plane rather than a single point. Such bars are superimposed on the theoretical predictions of Equation (12) in Figure 24. The experiment is lower than the theory by a factor of about 2; however, the absence of information on the unit Reynolds number effect leaves this comparison unsettled. For instance, if P_o in the present test could have been raised by a factor of about 2, complete agreement between theory and experiment could result.

Figure 24 also shows the data of Birch and Keyes (Reference 3); the agreement with the theory is excellent. Figure 25 compares the theory (with $\lambda = 1$ in Equation (12)) with the data of Crawford (Reference 9). The agreement is more than satisfactory even though Crawford's unit Reynolds number effect casts his data, too, in the form of vertical bars.

It is obvious from the above that the theory does a creditable job in predicting the vicinity where the transition zone would occur in a shear layer. Considering the range of data (M_1 from 2 to 6, λ from 0.04 to 1) the comparisons made attest to a large improvement which the present theory causes to the state of the art. We should stress, of course, that factors of 2 are common errors in transition measurement as well as in the definition of what transition is. But even more important, the qualifications to the theory (Section 1.2.5) should be kept in mind. It is indeed surprising that the theory does as well as it does with the sparse information necessary for its formulation.

1.6 CONCLUSIONS

1. An analytic expression has been derived for predicting the onset of transition in homogeneous free shear layers. This theory is based on physical principles, utilizes no adjustable constants, follows the author's conceptual approach for other flows (e.g. wakes), and divulges the transition dependence on M_1, λ and T_{02}/T_{01} for the first time. The results support qualitatively the earlier empirical ideas of the dependence on M_1 and λ; transition is found to move downstream as T_{02}/T_{01} is increased.

2. An experiment was done to enrich the data base with which the above theory can be compared. The test, designed to produce supersonic shear layers at a hitherto unexplored range of λ ($\lambda < 0.1$) achieved the designed flow conditions, although some portions of the matrix could not be utilized.

3. The agreement between the new test data and the theory is good; the expected large downstream movement of X_T with greatly decreased λ was found, although there is still a numerical disparity by a factor of about 2. Earlier data from two other sources show very good agreement with the theory.

4. A strong dependence of X_T on the unit Reynolds number has been found in the new as well as in the old data, which cannot be rationalized, and which is not accounted for in the theory.

1.7 RECOMMENDATIONS

The following is recommended, based on the discussion of the theory and on the conclusions just drawn:

a. Continue the development of the transition prediction formula, Equation (12), with the purpose of explaining the observed dependence on unit Reynolds number.

b. Extend the theory to inhomogeneous mixing layers (different gases).

c. Experimentally, verify the observed unit-Reynolds-number dependence under the same test conditions, but utilizing an alternate transition detector, e.g. the hot-wire anemometer.

d. Obtain FSL transition data for regimes not probed so far (e.g. for $0.1 < \lambda < 0.2$, or $M_1 > 5$ or both).

e. Measure the turbulence intensity u' and scale length Λ for any feasible combination of λ and $M_1 > 1$.

PART II
DENSITY FLUCTUATIONS IN COOLED SUPERSONIC WAKES

2.1 SUMMARY

An experiment was conducted for the dual purpose of measuring the influence of nozzle-cusp cooling on its wake in a simulated gas-dynamic-laser cavity, and of evaluating a new technique of measuring turbulent fluctuations. The turbulent nozzle-cusp wake was probed with a dynamic pitot tube which exhibited the wideband response expected of a high-quality turbulence sensor. The density fluctuations detected as a function of cusp temperature agreed satisfactorily with theoretical predictions.

2.2 PURPOSE

This author has published predictions of fluid behavior in supersonic wakes trailing gas-dynamic-laser nozzle cusps (References 17 and 18). These predictions address the laminar wake as well as the mean and fluctuating flow in cases where the wake is turbulent. Verification of this theory by experiment is important because of its good potential as a design tool for GDL cavities. In general, the agreement between this theory and the experimental data on the mean wake flow of Peterson and this author (References 19 and 20) is adequate but no measurements of the wake turbulence in GDL wakes has been reported so far. Some such data are reported here.

2.3 EXPERIMENT DESIGN AND TEST SET-UP

The turbulent wake density fluctuations ρ' were chosen for measurement from among the many possibilities partly since these fluctuations are explicitly predicted in Reference 18 and partly because of their practical importance to the GDL cavity flow. Specifically, the object was to determine the effect of cusp cooling on ρ', an effect which the theory of Reference 18 treats at some length. The test set-up was identical to that of Reference 20, using the same triple nozzle array described in that reference. In this arrangement, sketched in Figure 26, three continuous streams of air flow each at nominal $M = 4$, generated at $P_o = 755$ mm Hg and $T_o = 606°R$, are separated by the two-dimensional wakes shed by the trailing edges of the two nozzle cusps. Detailed quantitative description and other characteristics of this set-up are given in Reference 20 and will be omitted here for brevity.

The wake examined here was that of the upper cusp (Figure 26) which can be cooled internally by circulating LN_2. Various levels of the cusp wall temperature T_w can be achieved by throttling the coolant. As mentioned in Reference 20, cooling below $T_w \simeq -50°F$ is possible but impractical because tiny ice particles then form on the throat region of the cusp which greatly distort the flow. In this test, measurements of ρ' were made at $T_w = -40°$, 0°, 40°, 90° and 126°F.

Since Reference 20 indicates that both wakes were found laminar, or transitional at best, steps were taken to ensure turbulence in the wake of the upper cusp by tripping its boundary layer. This was done by completely covering all its wetted surfaces with No. 60 grit deposited on a thin epoxy

layer. This scheme was successful and the upper wake was completely turbulent, as desired. Thus, the effect of T_w on the density fluctuations of a turbulent wake could be studied.

2.4 PRINCIPLE OF MEASUREMENT

In order to avoid the fragility problems and protracted data reduction operations with the hot wire anemometer, this measurement of ρ' put to test a novel approach to turbulent diagnostics, which is the dynamic pitot probe. This probe has been used elsewhere in the past only in a qualitative way and without the benefit of a rationale for its use. This rationale, given by this author recently (Reference 21), is as follows. The instantaneous fluctuation Δp_T of the pitot pressure p_T is a function of the corresponding fluctuations Δp and ΔM of the static pressure p and Mach number M, respectively:

$$\frac{\Delta P_T}{P_T} = \frac{\Delta P}{p} + \left(7 - \frac{35M^2}{7M^2-1}\right) \frac{\Delta M}{M} \qquad (18)$$

for $\gamma = 1.4$; here Δp_T, Δp and ΔM stand for time functions, not rms or averaged quantities. For $M > 2$, the parenthesis in Equation (18) becomes 2, and if the equation of state

$$\frac{\Delta p}{p} = \frac{\Delta \rho}{\rho} + \frac{\Delta T}{T} \qquad (19)$$

is also used, Equation (18) gives

$$\frac{\Delta p_T}{p_T} = \frac{\Delta \rho}{\rho} + 2\frac{\Delta u}{u} \qquad (20)$$

The presence of the velocity fluctuations $\Delta u/u$ in (20) can now be eliminated via two assumptions. One is the "standard" assumption of hot wire anememetry:

$$\frac{\Delta p}{p} = 0 \;, \quad \frac{\Delta \rho}{\rho} = -\frac{\Delta T}{T} \qquad (21)$$

The second assumption utilizes the author's consistent finding (References 22 and 23) that in supersonic wakes, even with heat transfer, the velocity and temperature fluctuation are anti-correlated:

$$\frac{\Delta T}{T} = -(\gamma-1)\, M^2 \frac{\Delta u}{u} \qquad (22)$$

Inserting (21) and (22) into Equation (20), we find the gas density fluctuation in terms of the pitot pressure fluctuations:

$$\frac{\rho'}{\rho} = \frac{1}{1 + \frac{2}{(\gamma - 1)\, M^2}} \qquad \frac{P_T'}{P_T} \tag{23}$$

where primes, indicating rms values, have now replaced the instantaneous values Δp_T, etc. The assumptions underlying Equation (23), mentioned above, are quite safe for the present purposes and this equation, therefore, formed the basis for the present fluctuation measurement.

2.5 METHOD OF MEASUREMENT

According to Equation (23), the desired goal of this test, i.e., the normalized density fluctuations ρ'/ρ, can be found if one can measure the normalized pitot pressure fluctuations p'_T/p_T and the local Mach number. Measurement of p'_T, however requires a sensor of proper spatial and temporal resolution. For spatial resolution, a sensor size on the order of 5% of the wake width b is needed or about 0.1 cm since $b \simeq 2$ cm. For temporal resolution, a basic rule requires a frequency response extending to $10u_\infty/b$ or higher; since the flow velocity is on the order of 7×10^4 cm/sec (Reference 20) the response should extend at least to 350 KHz.

Until recently, pressure sensors meeting these requirements were difficult to find. A relatively modern transducer development, the Kulite Model CQL-030-100, was chosen for the present work. The face diameter of this sensor, 0.087 cm, falls within the size requirement quoted above. The reference end of this differential transducer was hermetically sealed at 1 atmosphere, and the sensor was repeatedly calibrated in the range 0 - 400 mm Hg. abs. This is a small fraction of the transducer 100 psi range but the response was, nevertheless, found to be quite linear. Calibration was made easier by placing the transducer permanently with its tip protruding from the front of a cylindrical holder and by fitting a suction cup over the end of the holder whenever calibration was desired. Since frequent calibrations were needed, this scheme made them possible with a minimum of effort.

Typical calibrations of the transducer are shown in Figure 27. For any single calibration the output, in mv, is related to the pressure in mm Hg by

$$p_{mv} = A + Bp_{mm} \tag{24}$$

The "zero shift" A was found to vary from one calibration to the next, making this transducer unreliable for absolute pressure measurements. The factor B, however, remained the same within very few percent; since the fluctuations Δp_{mv} and Δp_{mm} are by the differential calculus related through

$$\Delta p_{mv} = B \Delta p_{mm}, \quad p'_{mv} = Bp'_{mm} \tag{25}$$

it follows that once the rms voltage output fluctuations p'_{mv} are measured, the fluctuations in pitot pressure can be deduced. The factor B was found to be close to 0.0067. Together with Equation (23), Equation (25) completes the formulas needed to find the gas density fluctuations from the measured pitot tube voltage fluctuations.

By Equation (23), the local mean Mach number is also needed, which was previously found by measuring separately the local static and pitot pressures (Reference 20). For expediency, in the present test the mean pitot pressure was first recorded in the inviscid flow between the two wakes and combined with p_o to give the local wake edge Mach number, and thus the wake edge static pressure p. Using the finding of Reference 20 that p was uniform across the wake, it was next assumed that this p was the same on the wake centerplane. The measurement of p_T on the centerplane, and its combination with p, thus produced M = M(0) on the centerplane for insertion in Equation (23). (Note that all ρ'/ρ data taken in this test were measured on the centerplane). In the beginning, it appeared logical to use the same Kulite transducer to take these two values of p_T; however, this was impossible since, as mentioned above, the erratic values found for A in Equation (24) made this transducer impractical for such mean (steady state) measurements. These two p_Ts were, therefore, measured with an ordinary flattened pitot tube.

2.6 EXPERIMENT GEOMETRY

The scope of this test was limited to the measurement of ρ'/ρ on the centerplane of the turbulent wake for the few temperature ratios T_w/T_o mentioned in Section 3. The dynamic transducer was placed at x=5.8" (14.7 cm) ($\Delta x/h_1$=8) downstream of the trailing edge of the upper nozzle cusp which, as noted earlier, was roughened to trip its boundary layer and to produce wake turbulence. The flow was continuous at P_o = 756 mmHg and T_o = 606°R. The probe tip lay on the wake centerplane and one rms voltage output for each T_w was recorded. After this was done, steady-state (mean) p_Ts were recorded at the same conditions by an ordinary pitot tube which was also used to measure wake-edge pitot pressures.

2.7 RESULTS

2.7.1 PERFORMANCE OF THE DYNAMIC PITOT PROBE

The dynamic pitot tube performed very well, giving a large a.c. output in the turbulence. The key criterion of its operation is its output spectrum, which is shown in Figure 28. As noted earlier, signals at frequencies of order 350 KHz were expected; as seen from the spectra, signals at frequencies as high as 640 KHz are detectable with little trouble. Furthermore, pressure transducers of this kind have a "flat" frequency response up to their resonance frequency; one advantage of the CQL-030-100 is that its resonance, in consequence to its small size, lies at 750 KHz. Thus, this transducer is not only amply sensitive to the p_T fluctuations, but has a flat frequency response (an advantage over the hot wire) over the entire frequency range of interest and freedom from contamination of its output by its resonance over that range.

2.7.2 DENSITY FLUCTUATIONS IN THE TURBULENT WAKE

Table VI shows the results of the quantitative measurements with the Kulite CQL-030-100. For nozzle temperature ratios from 0.69 to 0.96, the centerplane Mach number changes only slightly; its effect on the bracket of Equation (23), however, is sufficient to convert the undecisive variations of p_T' (from 8.5 to 9.3 mmHg rms in Table VI) to a clear variation of the density fluctuations ρ'/ρ.

The density fluctuation data on Table IV are plotted in Figure 29 together with the theoretical prediction taken from Reference 18. According to the theory, nozzle cooling suppresses ρ'/ρ by about 27% as T_w decreases from T_o to 0.6 T_o, and by about 19% in the range $0.69 < T_w/T_o < 0.96$. In the latter range, the data show about half this decrease and also lie about 30% below the theory.

It should be stressed, of course, that these are the first quantitative turbulence data reported in GDL turbulent wakes and the first, to this authors knowledge, showing the cooling effect on the fluctuations. At this stage, the numerical agreement between theory and experiment should, at the least, be considered satisfactory and the evidence of turbulence suppression by nozzle cusp cooling should be taken as conclusive.

2.8 CONCLUSIONS

1. A miniature pressure transducer, employed as a dynamic pitot tube, has been successfully used to directly measure density fluctuations in supersonic flow, with excellent sensitivity and frequency response. This performance, coupled with its great expediency in handling and signal interpretation, make this technique a serious rival to hot wire or hot film anemometry.

2. It has been verified that when a GDL nozzle cusp is cooled below the stagnation temperature, the density fluctuations on its turbulent wake centerplane decrease. Qualitatively and quantitatively, this decrease is similar to that expected by the theory presented by this author in an earlier publication.

2.9 RECOMMENDATIONS

Recommendations are offered here both as regards the dynamic pitot tube technique, and also as regards the measurement of turbulence in cooled wakes. The quantitative knowledge of turbulence "suppression" or "amplification" as the heat input varies, is a very important problem at this juncture. Since the particular wake generators used could not be cooled below a certain limit, it is recommended that the test set-up is changed to one where much lower values of Tw/To can be reached. Specifically, it is recommended that the test is repeated in the same wind-tunnel at Mach 3, but with the wake generator consisting of a thin circular tube. Passing any amount of LN_2 through this tube should be quite simple, and the Tw/To should reach considerably lower values than in the test discussed here.

Further experimentation with the dynamic pitot tube is strongly encouraged. This author considers this so important that he recommends separate funding of a program to measure density fluctuations with this instrument. Specifically, parallel measurements with this method and the hot-wire anemometer should be done, so that the density fluctuations can be simultaneously measured with these two methods for purposes of comparison.

TABLE VI

FLUCTUATION DATA

P_o = 756 mmHg. abs., T_o = 606°R, x = 5.8", $\Delta x/h_1$ = 7.9, y = 0

CASE	1	2	3	4	5
T_w (°F)	-40	0	40	90	122
T_w/T_o	0.693	0.759	0.825	0.907	0.96
p_T (0) (mm Hg)	58	60.7	58.9	57.1	51
M (0)	2.185	2.125	2.195	2.175	2.10
p_T' (0) (mm Hg)	8.58	9.36	9.36	9.36	8.58
ρ' (0)/ρ (0)	0.0722	0.0763	0.078	0.0797	0.0789

REFERENCES

1. Demetriades, A.: "Transition to Turbulence in Two-Dimensional Wakes", AIAA J., Vol. 16, No. 6, June 1978.

2. Demetriades, A.: "Interim Progress Report: Stability, Transition and Turbulence in Mixing Layers and Adjacent Streams", Aeronutronic Publication U-6488, Newport Beach, CA, October 1978.

3. Birch, S. F. and Keyes, J. W.: "Transition in Compressible Free Shear Layers", JSR Vol. 9, No. 8, p. 623, August 1972.

4. Ortwerth, P. J. and Shine, A. J.: "On the Scaling of Plane Turbulent Shear Layers", Laser Digest, AFWL-TR-77-118, p. 115, Spring 1977.

5. Oh, O. H.: "Analysis of Two-Dimensional Free Turbulent Mixing", AIAA Paper 74-594, New York, N. Y.

6. Demetriades, A.: "Turbulence Measurements in an Axisymmetric Turbulent Wake", Phy. of Fl. Vol. 11, No. 9, p. 1841, September 1968.

7. Laderman, A. J. and Demetriades, A.: "Mean and Fluctuating Flow Measurements in the Hypersonic Boundary Layer Over a Cooled Wall", JFM, Vol. 63, Part 1, p. 121, 1974.

8. Demetriades, A.: "Transition to Turbulence in Free Shear Layers", Aeronutronic Proposal No. P-24940 to AFOSR, 31 March 1978.

9. Crawford, D. H.: "Investigation of the Flow Over A Spiked Nose Hemisphere-Cylinder at a Mach Number of 6.8", NASA TN D-118, Washington, D.C. 1959.

10. Ikawa, H.: "Turbulent Mixing Layer Experiment in Supersonic Flow", Ph.D. Thesis, California Institute of Technology, Pasadena, CA 1973.

11. Laderman, A. J. and Demetriades, A.: "Investigation of the Structure of a Cooled-Wall Turbulent Supersonic Boundary Layer", Aeronutronic Publication No. U-6370, October 1977.

12. Demetriades, A.: "The Crocco Relation in Wake Flows", unpublished, 1979.

13. Shang, J. S. and Hankey, W. L. Jr.: "Numerical Solution for Supersonic Turbulent Flow over a Compression Corner", AIAA J., vol. 13, No. 10, p.1368, October 1975.

14. Reeves, B. and Todisco, WADC/ARL Report, 1969.

15. Beale, D. K. and Donaldson, J. C.: "Investigation of a Free Shear Layer Generated by Planar Shock Wave Intersection at Free-Stream Mach Number 8", AEDC-TSR-79-V30, AEDC, May 1979.

16. AEDC Staff: "Test Facilities Handbook", Tenth Edition, VKF, No. 3., AEDC, Tallahoma, Tennessee, May 1974.

17. Demetriades, A.: "Linearized Analysis of Gas Dynamic-Laser Wakes with Applications", J. of Energy, Vol. 1, No. 2, p. 73, March-April 1977.

18. Demetriades, A.: "Turbulent Fluctuations in the Wakes of Gas Dynamic-Laser Cusps", J. of Energy, Vol. 2, No. 2, p. 124, March-April 1978.

19. Peterson, Carl., Sandia Corporation, Private Communication, 1976-1978.

20. Demetriades, A.: "Experimental Test of the Theory of Multiple-Nozzle Cusp Wakes", Aeronutronic Report No. U-6395, December 1977.

21. Demetriades, A.: "Probes for Multivariant Flow Characteristics", Dynamic Flow Conference 1978, Marseille/Baltimore, September 1978.

22. Demetriades, A.: "Turbulence Measurements in a Supersonic Two-Dimensional Wake", Physics of Fluids, Vol. 13, No. 7, p. 1672, July 1970.

23. Demetriades, A.: "Final Report, Wake Structure Measurements, Advanced Penetration Problems", SAMSO TR 70-58.

24. Shapiro, A.: "The Dynamics and Thermodynamics of Compressible Fluid Flow", Vol. II, The Ronald Press Co., New York, 1954.

25. Korst and Chow: "ASME Paper", No. 70-WAIFE-12.

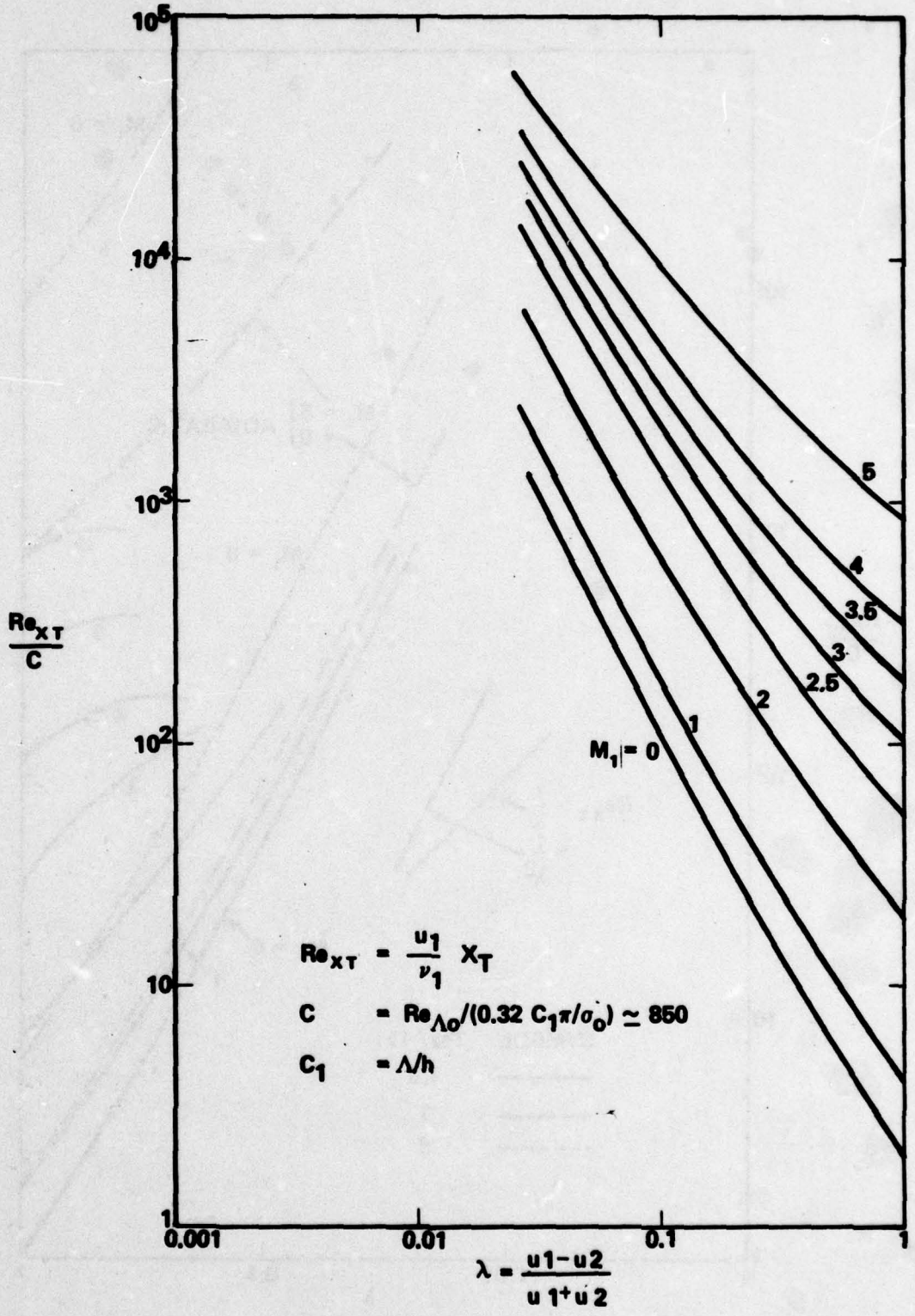

FIGURE 1. The predictions of Equation (9) for homogeneous adiabatic free shear layers in air.

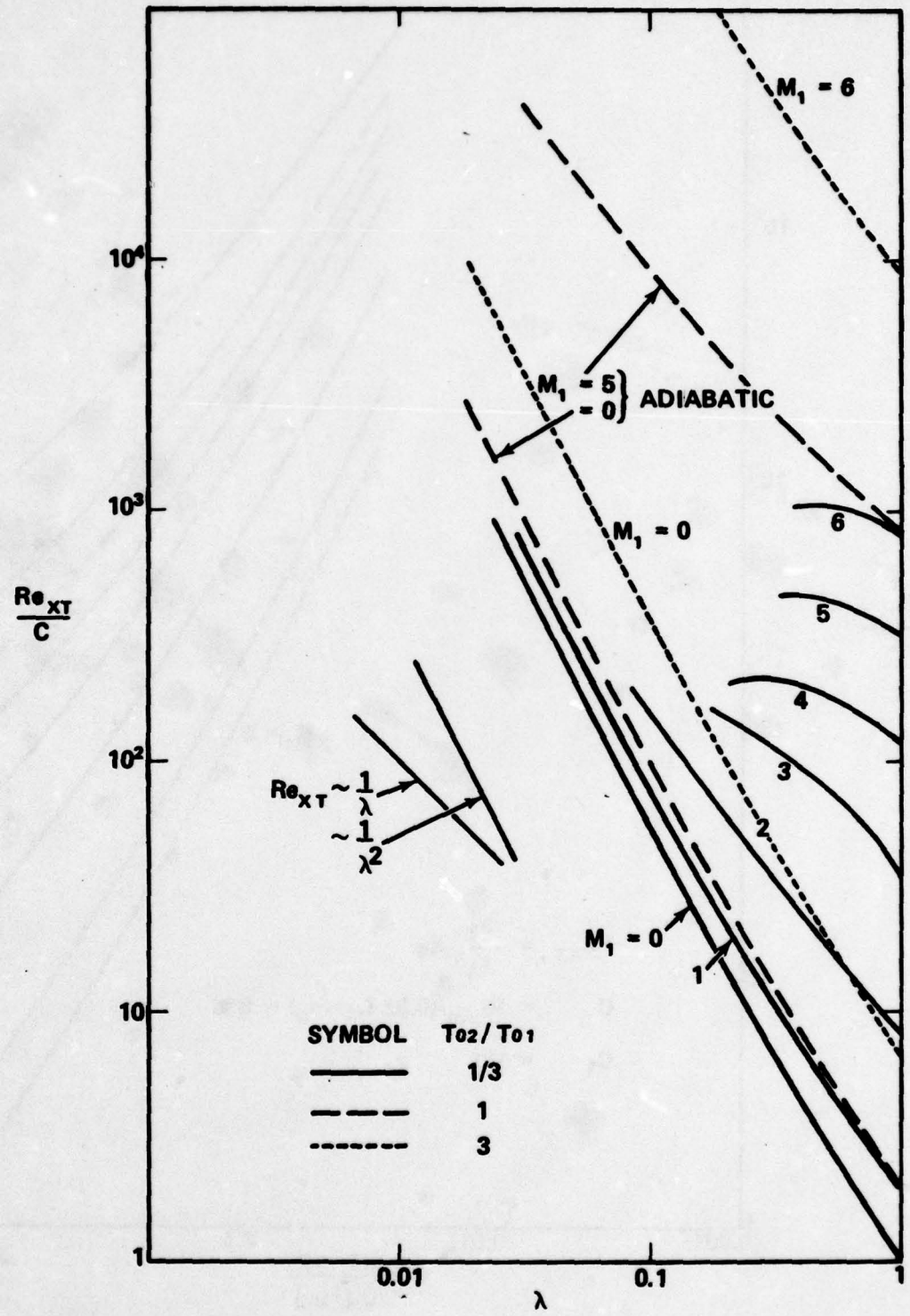

FIGURE 2. The predictions of Equation (9) for free shear layers in air, with heat transfer.

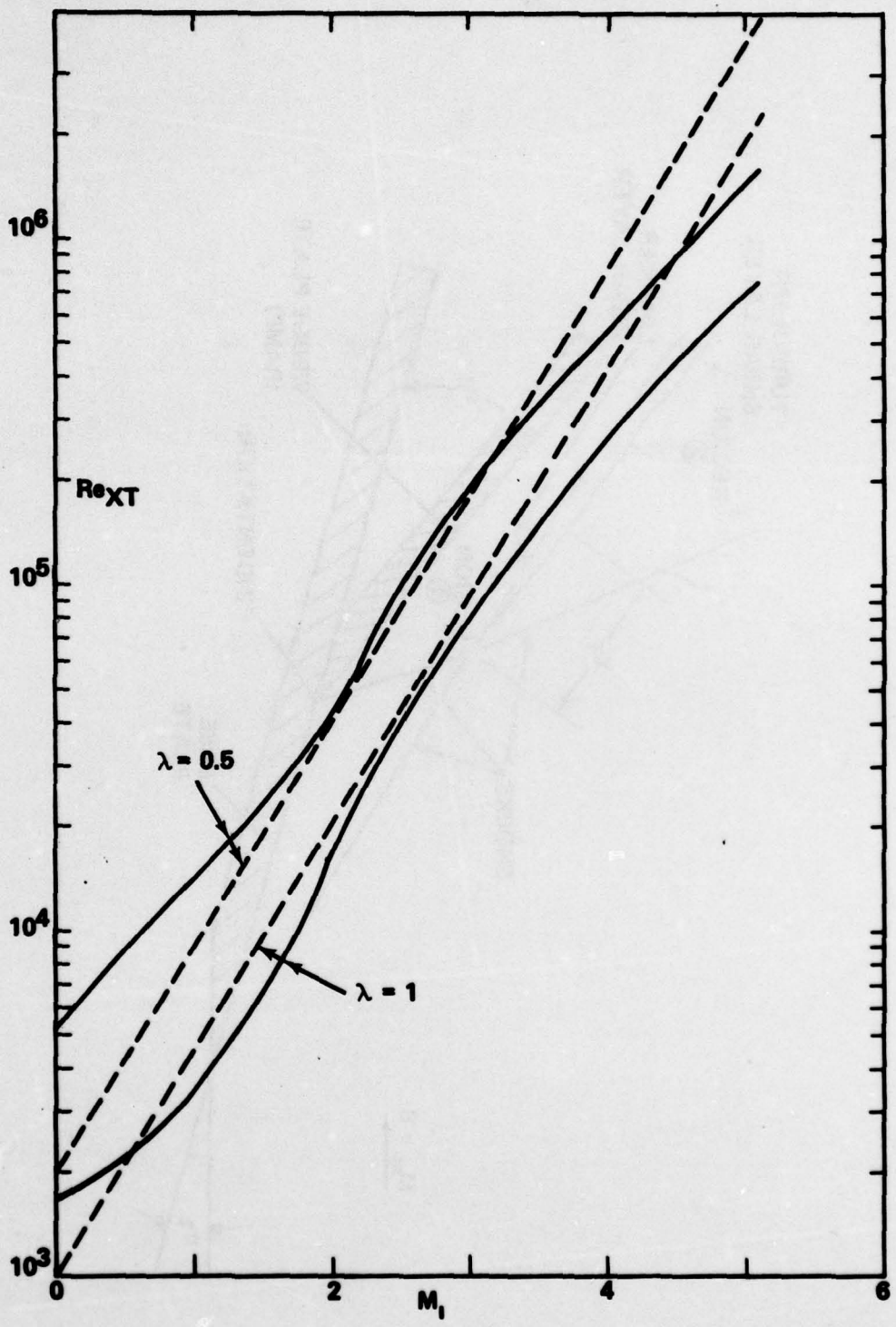

FIGURE 3. Comparisons of present theory (solid lines) with earlier data (dashed lines), as correlated by a previous formula.

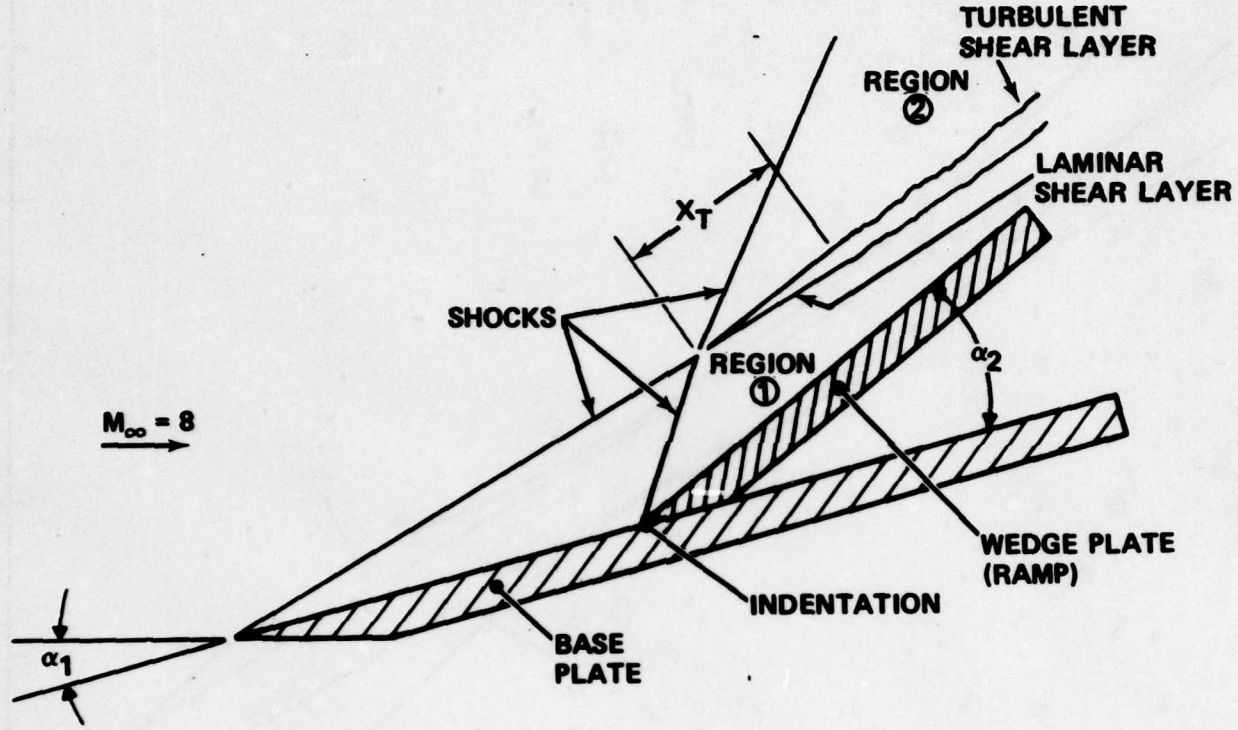

FIGURE 4. Schematic of the model and flow regime nomenclature.

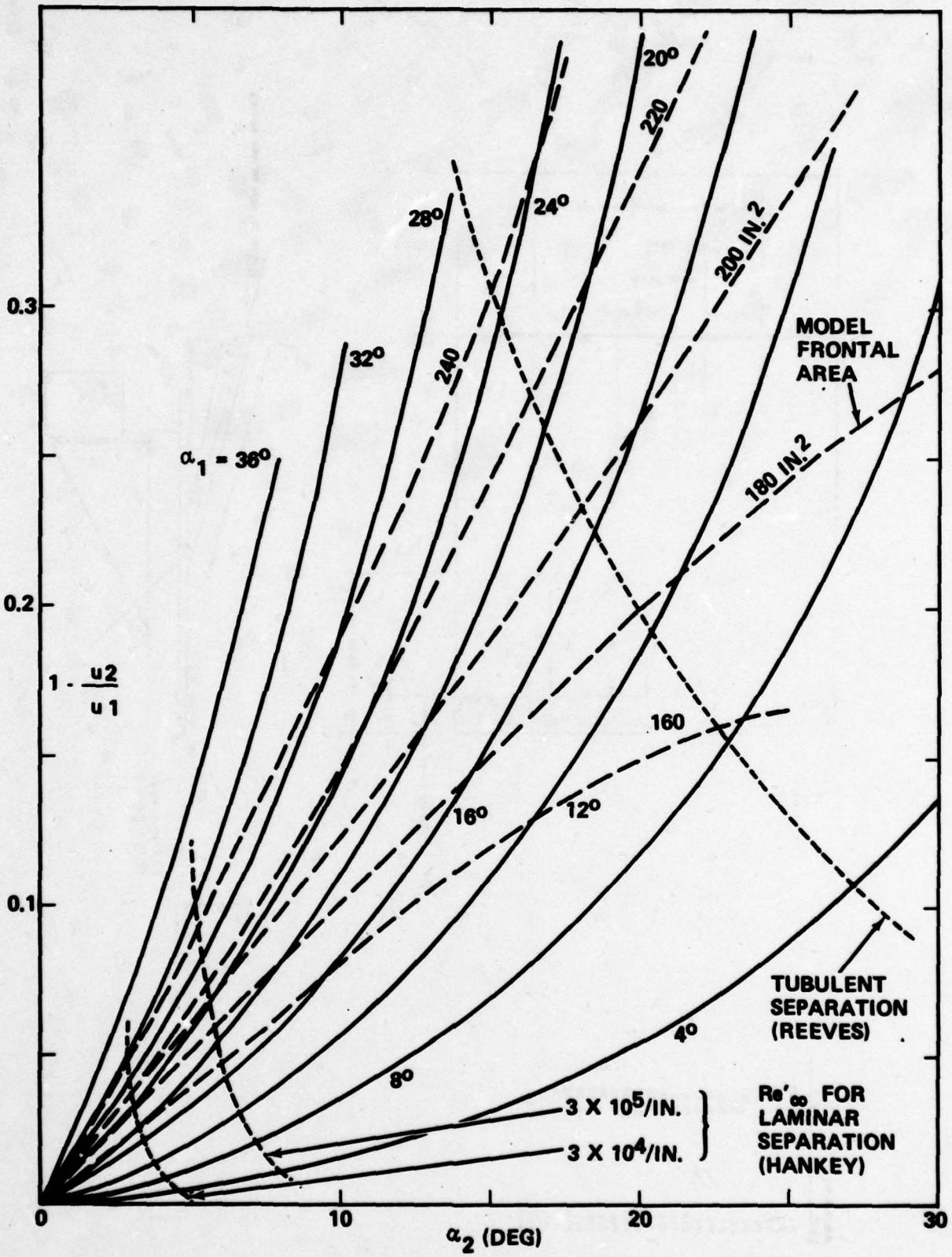

FIGURE 5. The expected FSL strength generated by the angles of α_1 and α_2, including the model frontal area and the maximum angles of α_1 and α_2 before separation occurs at the indentation.

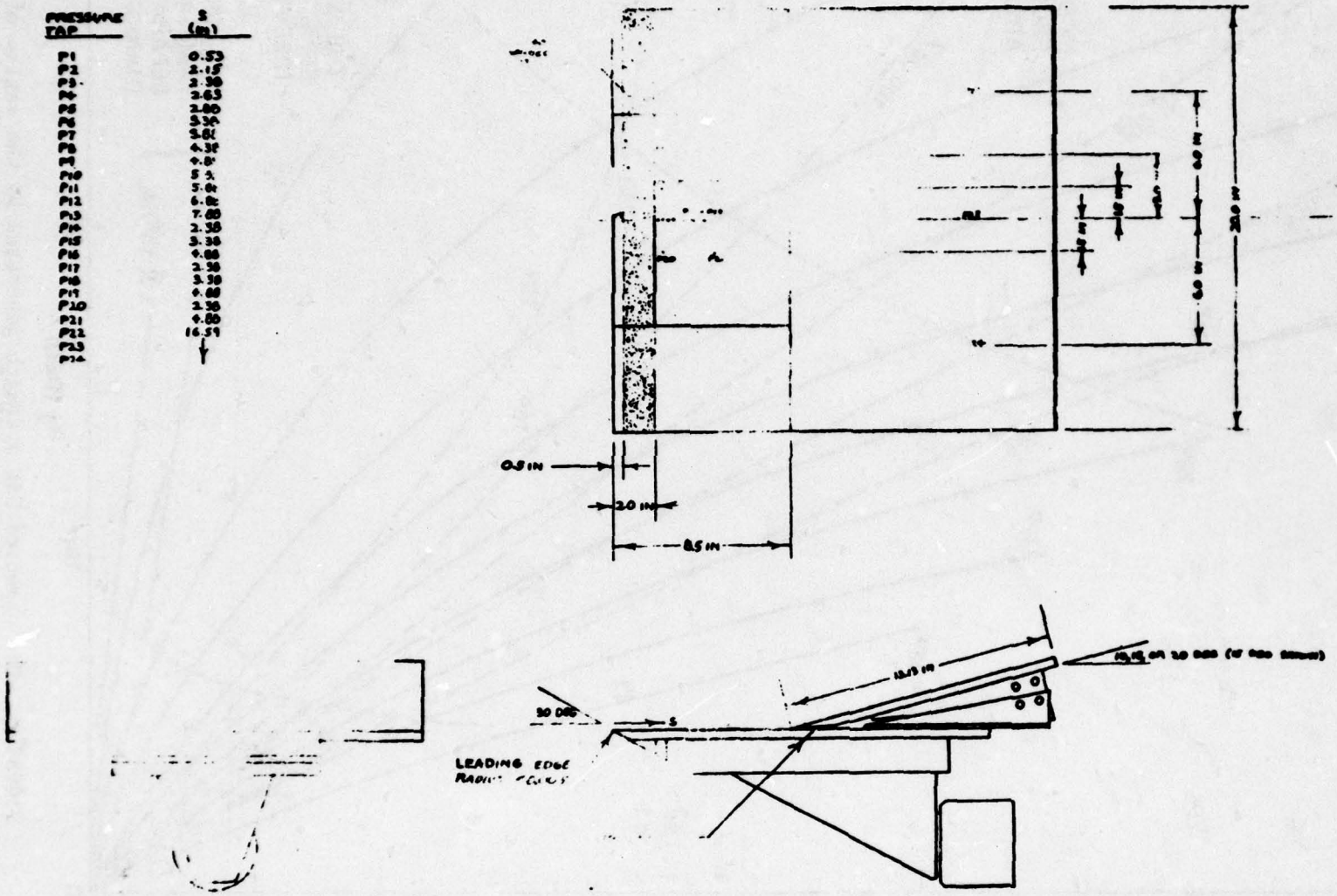

FIGURE 6. Dimensional drawing of the model.

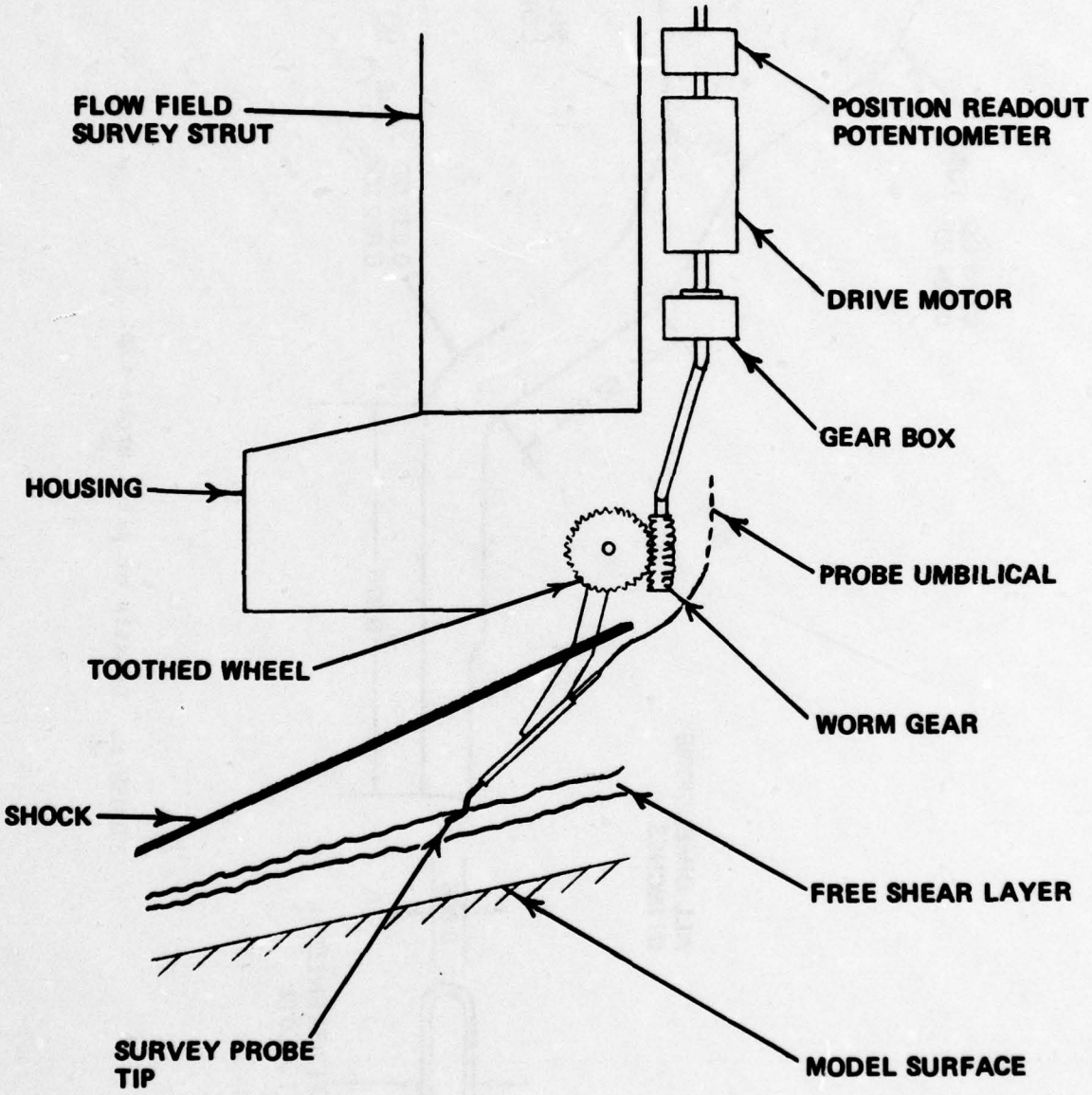

FIGURE 7. Schematic of the actuator and pitot probe placement.

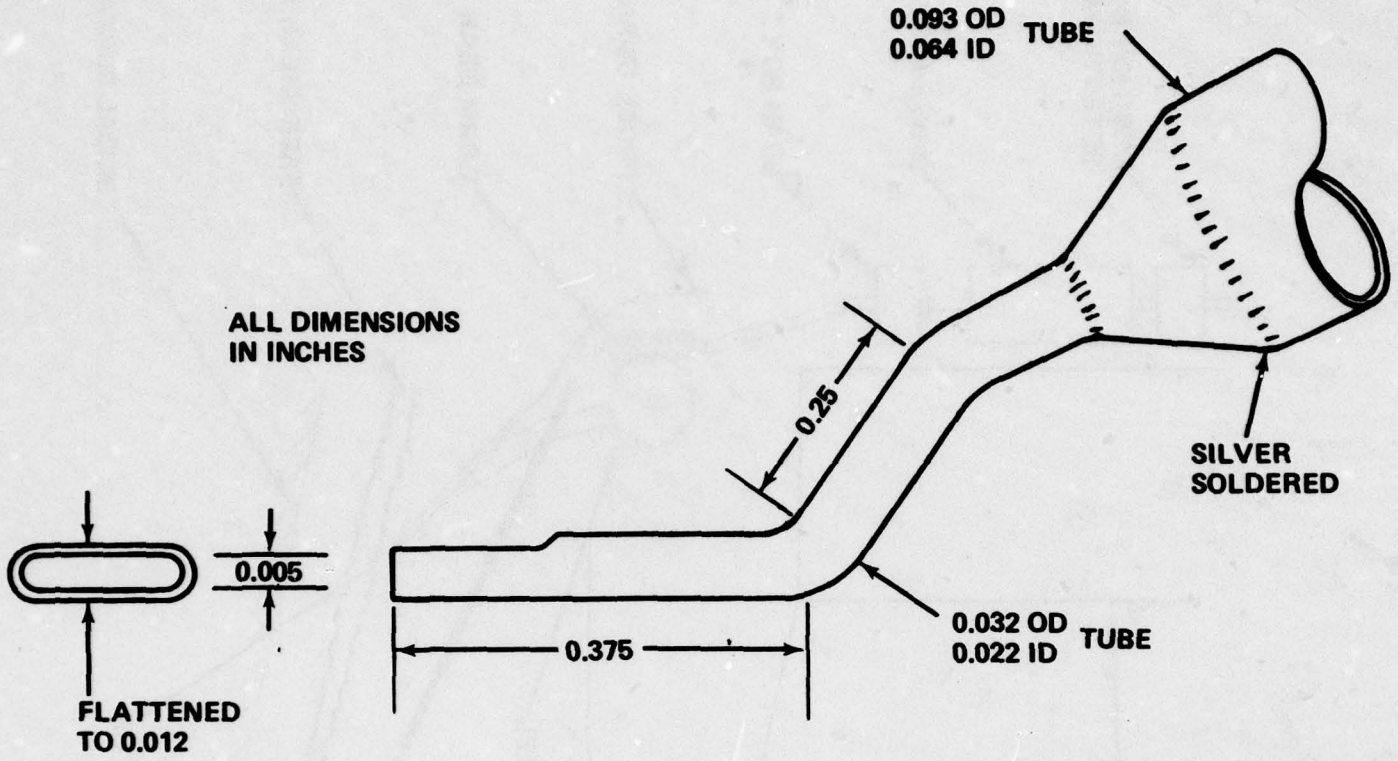

FIGURE 8. Details of pitot probe tip.

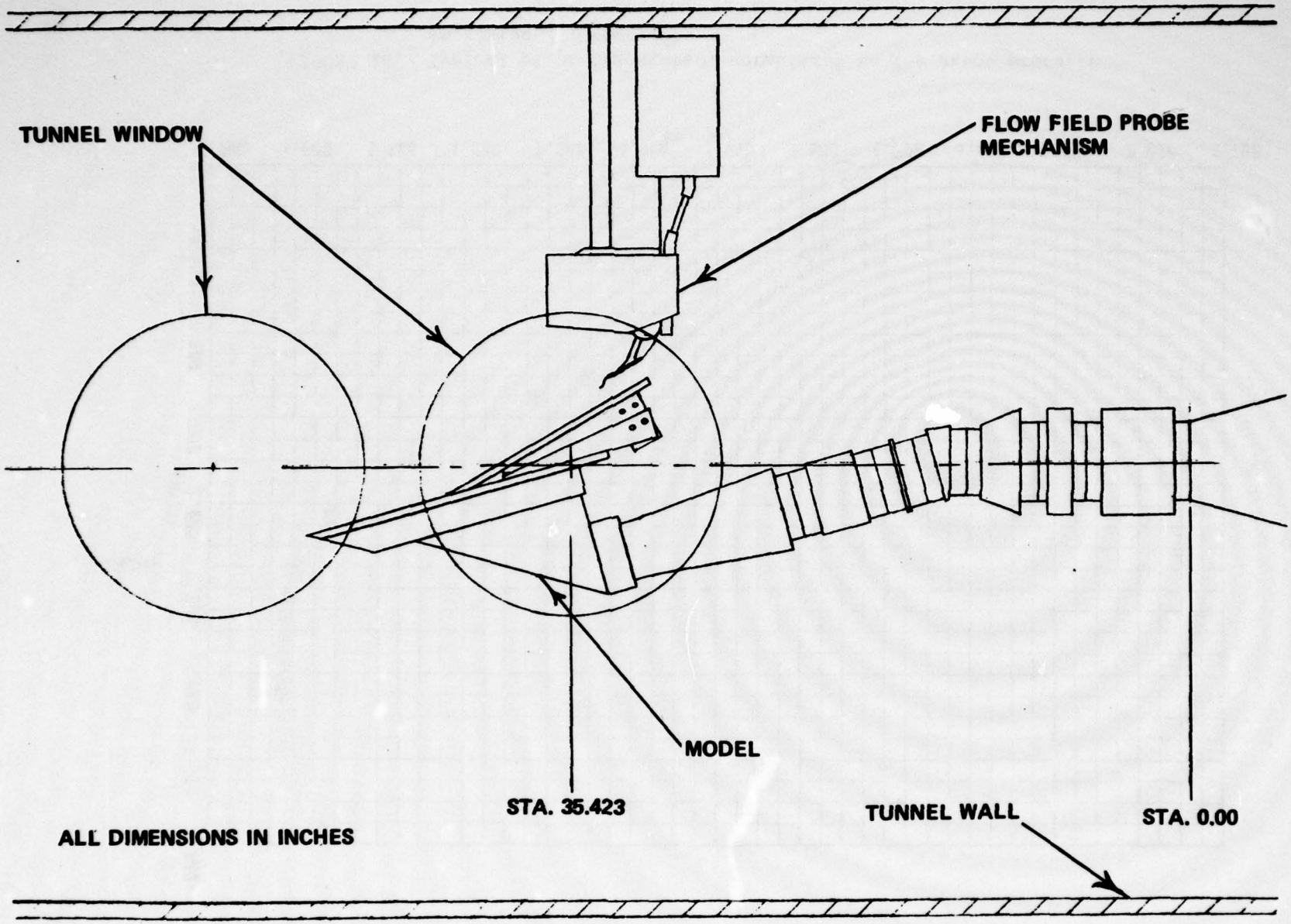

FIGURE 9. Placement of the model and overhead probe relative to the tunnel windows.

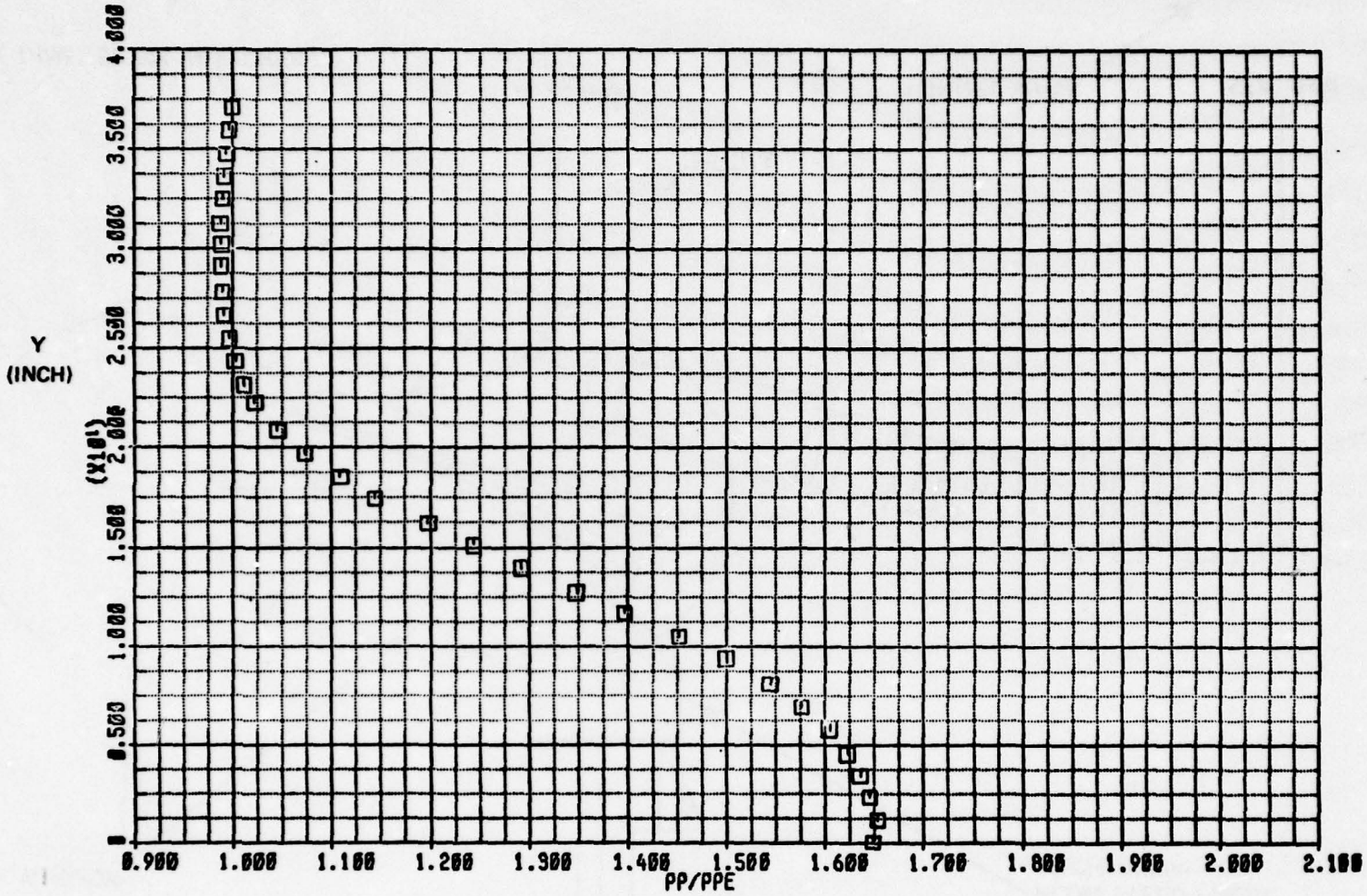

FIGURE 10. Typical pitot transverse, normalized to the pitot pressure in region 2 (Group 35).

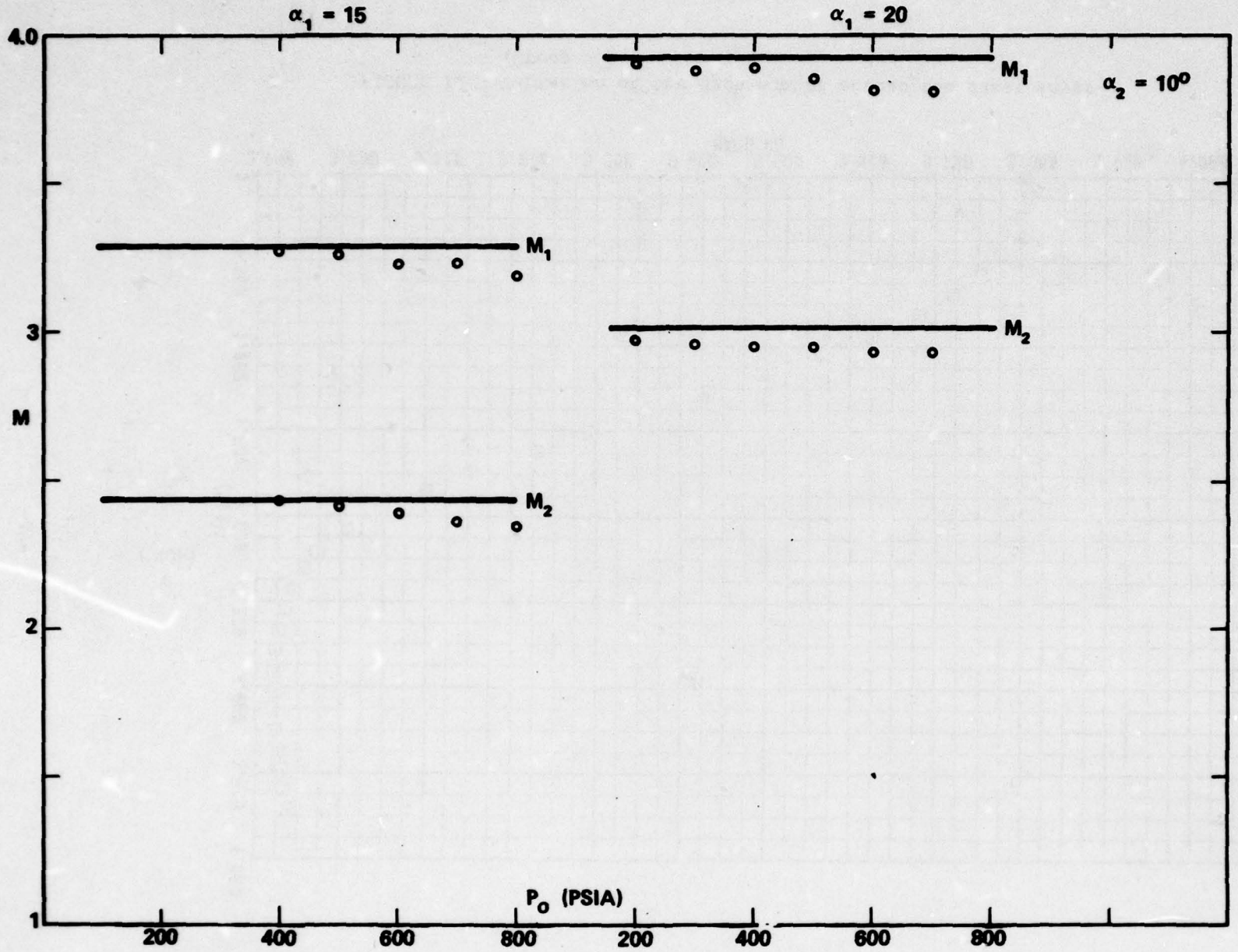

FIGURE 11. Variation of M_1 and M_2 as measured for the two design configurations $\alpha_1 = 15^o$, $\alpha_2 = 10^o$ and $\alpha_1 = 20^o$, $\alpha_2 = 10^o$. Solid lines represent the design expectations.

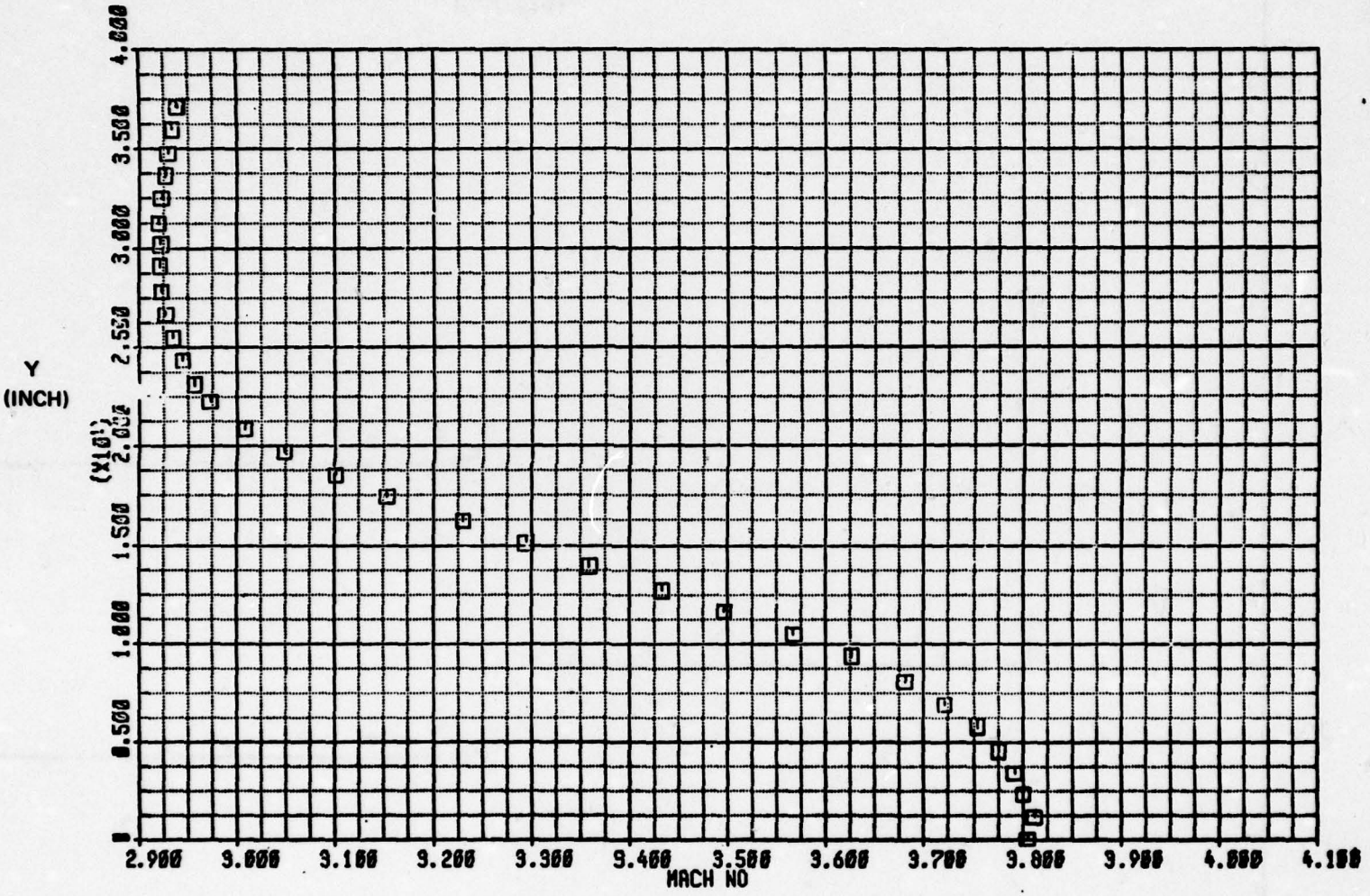

FIGURE 12. Variation of the Mach number across the shear layer (Group 35).

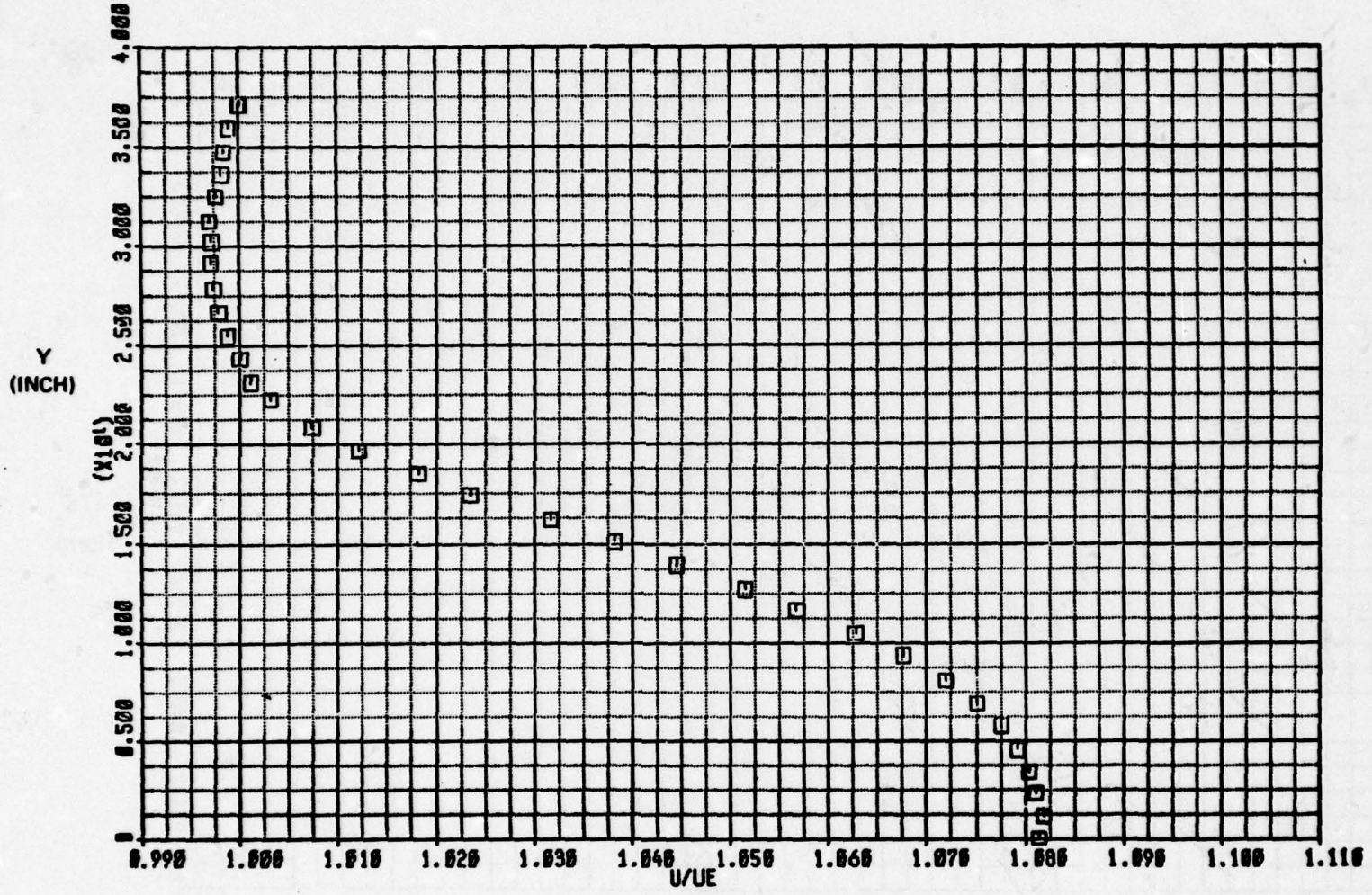

FIGURE 13. Variation of the velocity across the shear layer, normalized with the velocity in region 2 (Group 35).

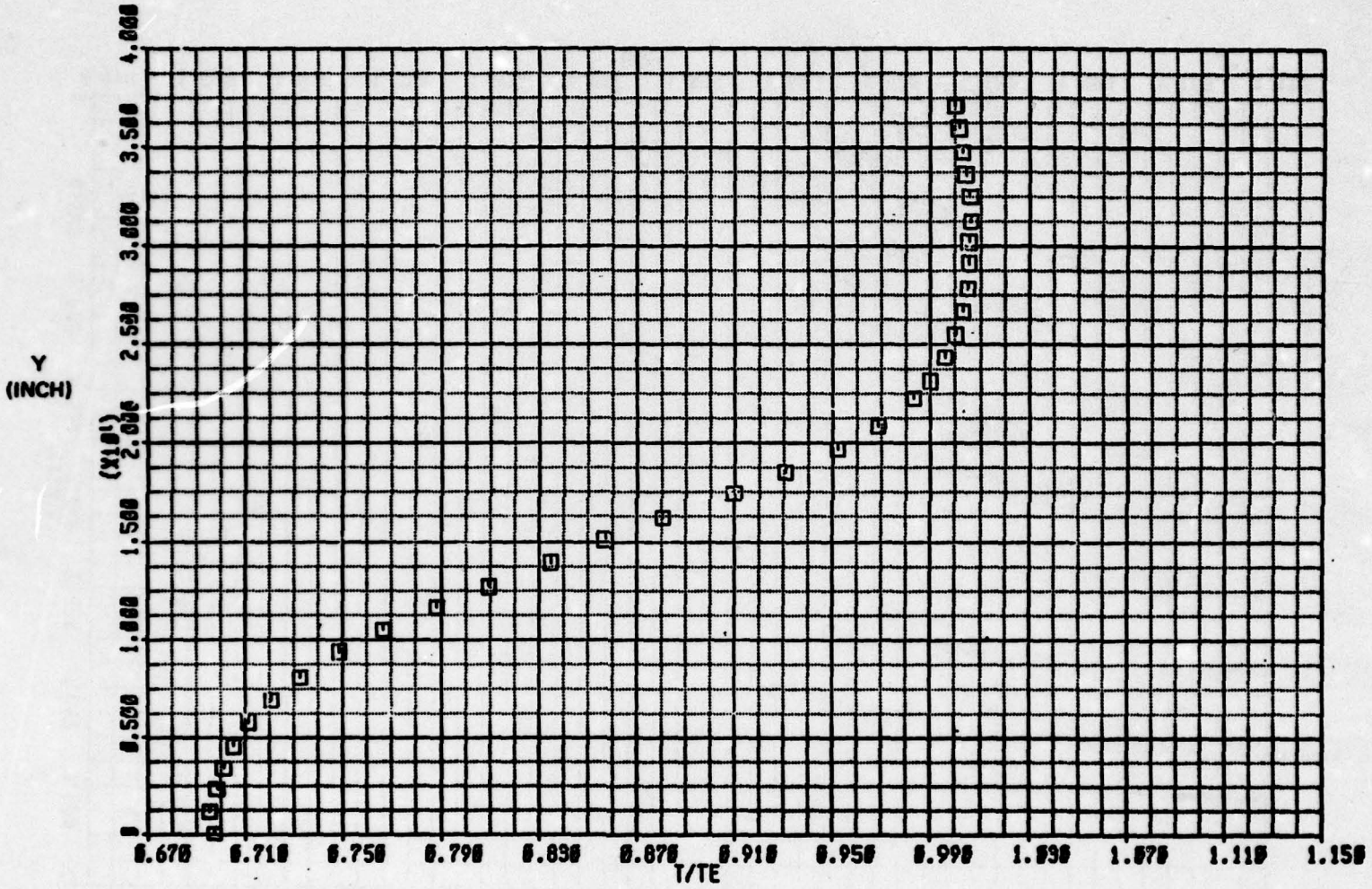

FIGURE 14. Variation of the static temperature across the shear layer, normalized with the temperature in region 2 (Group 35).

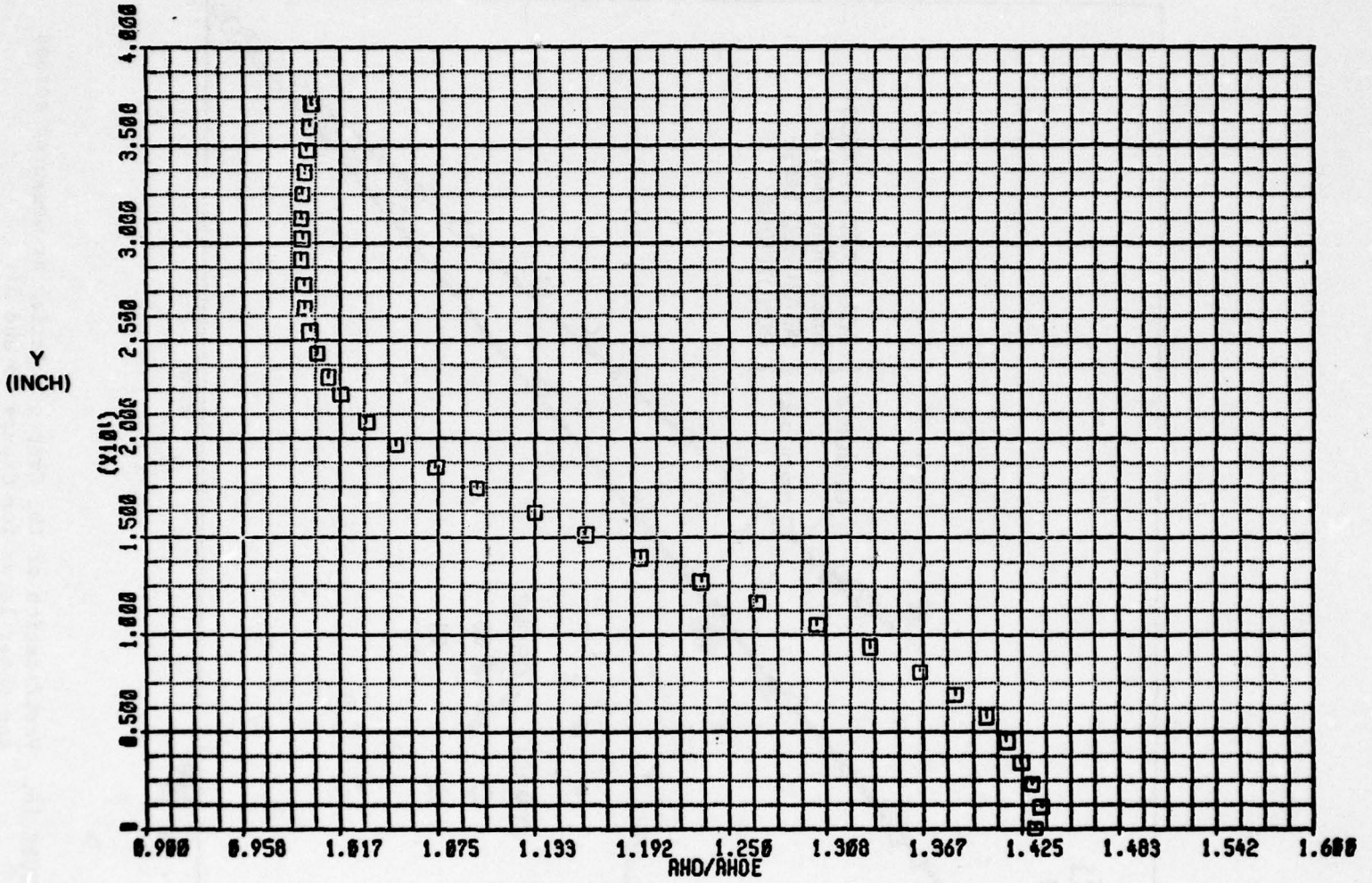

FIGURE 15. Variation of the density across the shear layer, normalized with the density in region 2 (Group 35).

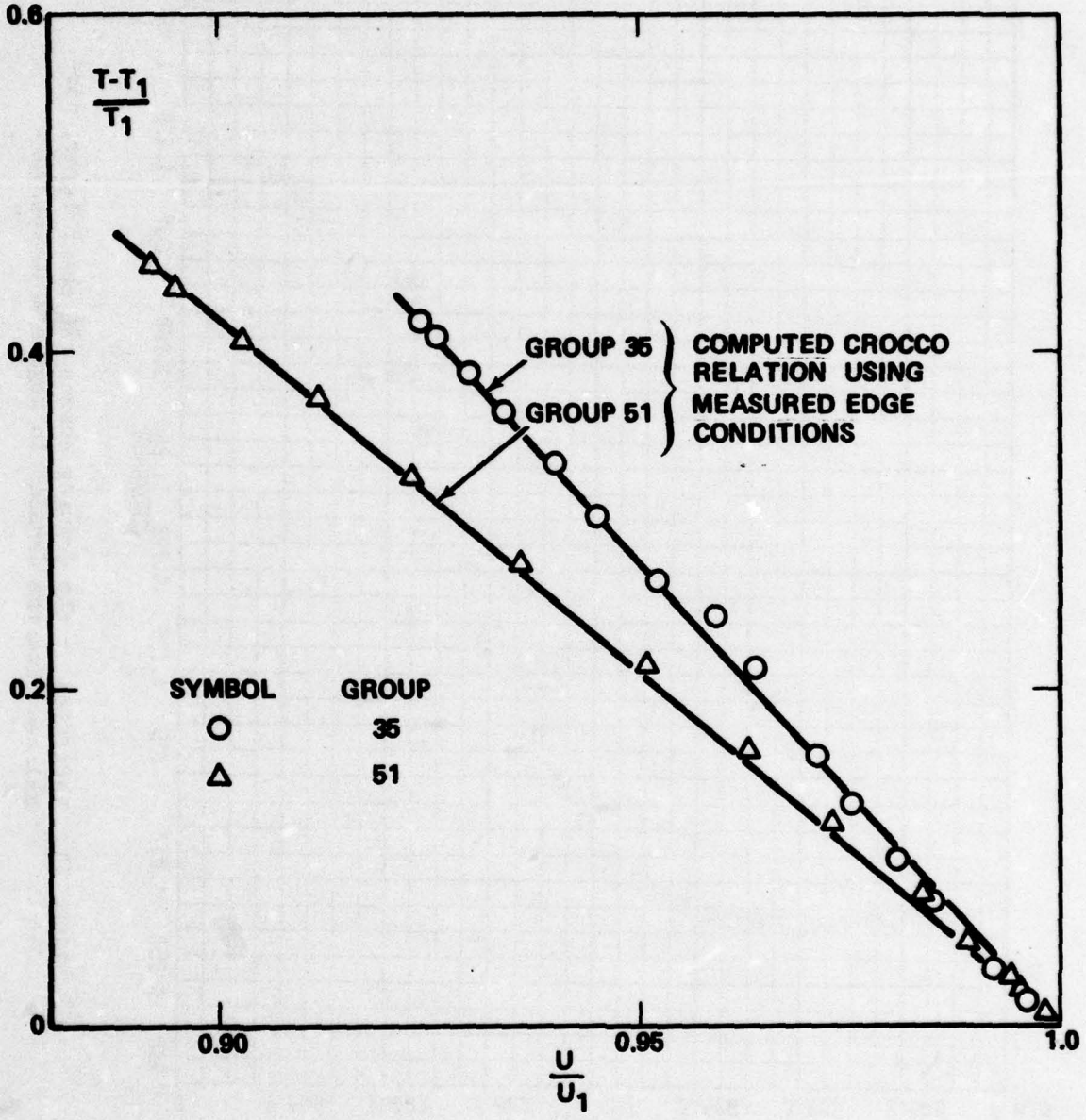

FIGURE 16. Verification of the Crocco relation as measured across the shear layer for Groups 35 and 51.

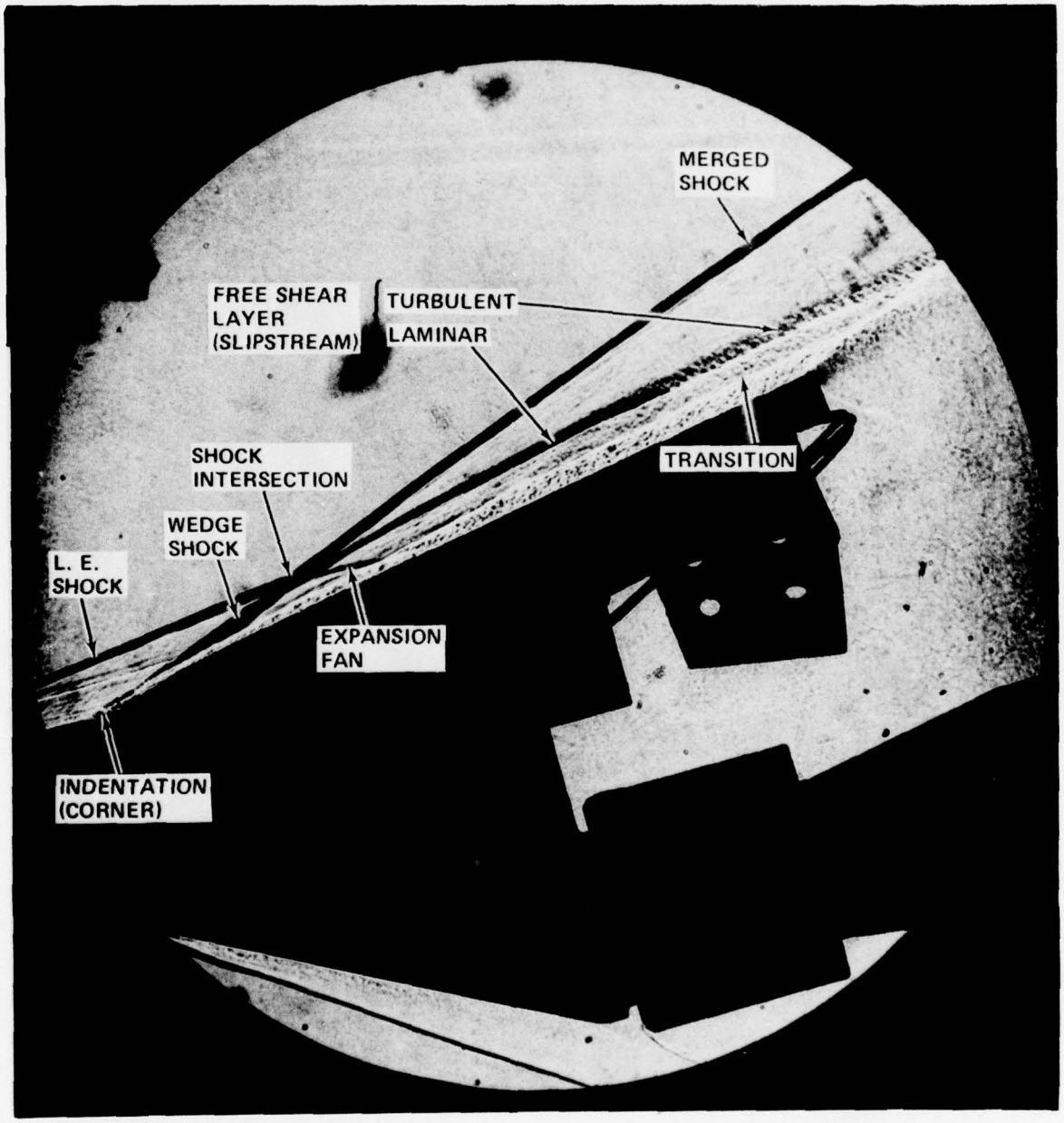

FIGURE 17. Spark shadowgram of the flow.

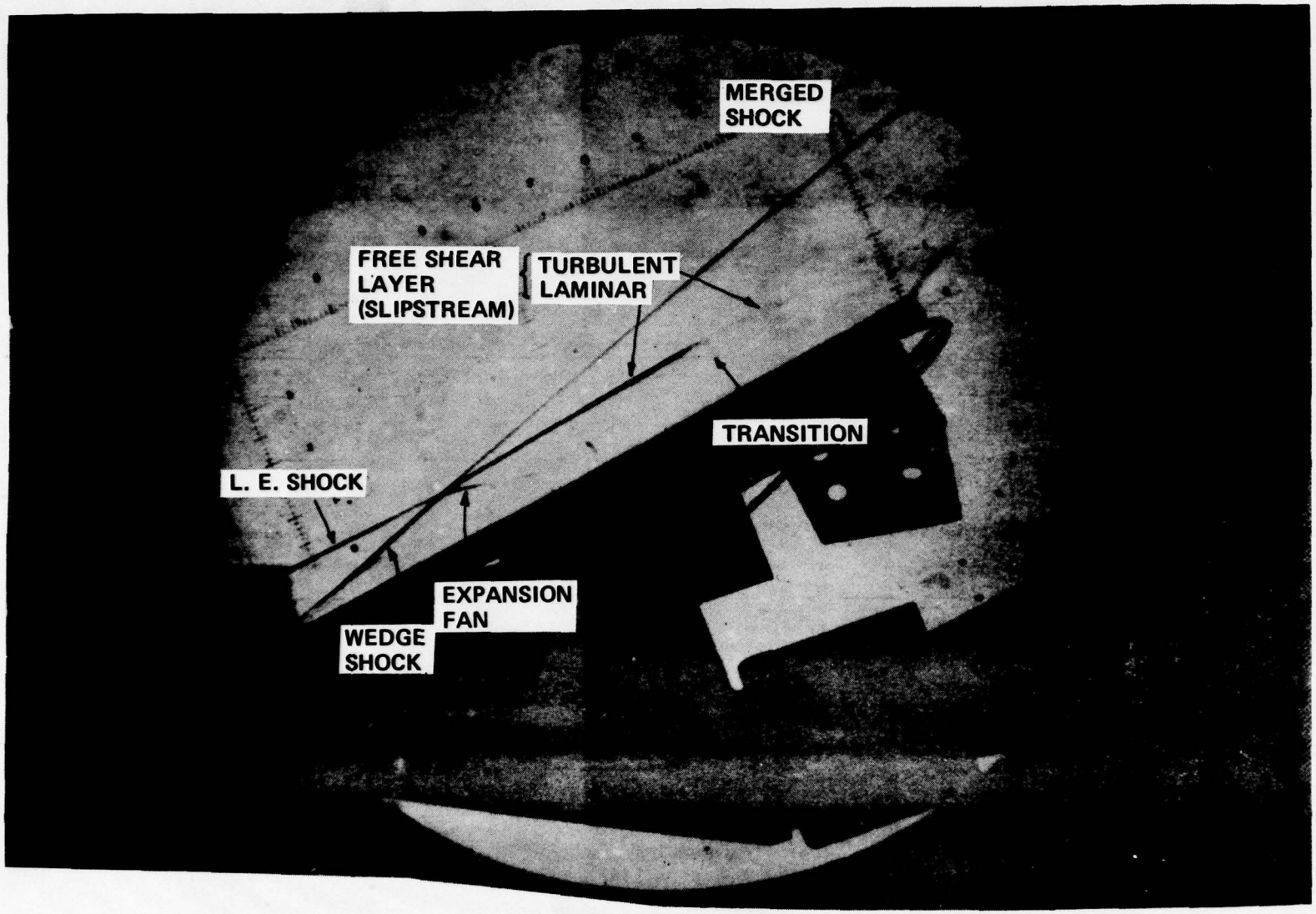

FIGURE 18. Time exposure of the flow.

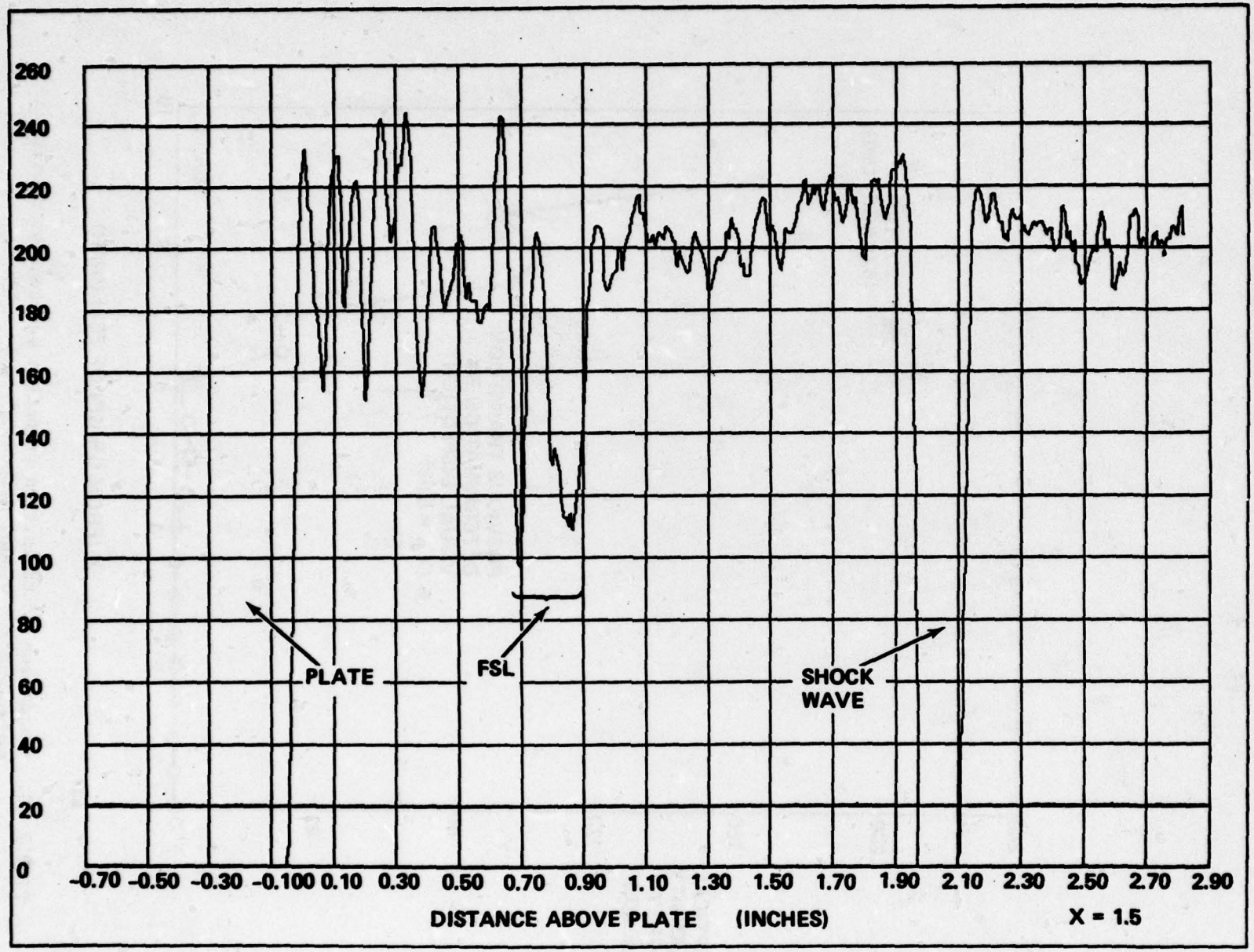

FIGURE 19. Densitometer trace across the flow (Group 1).

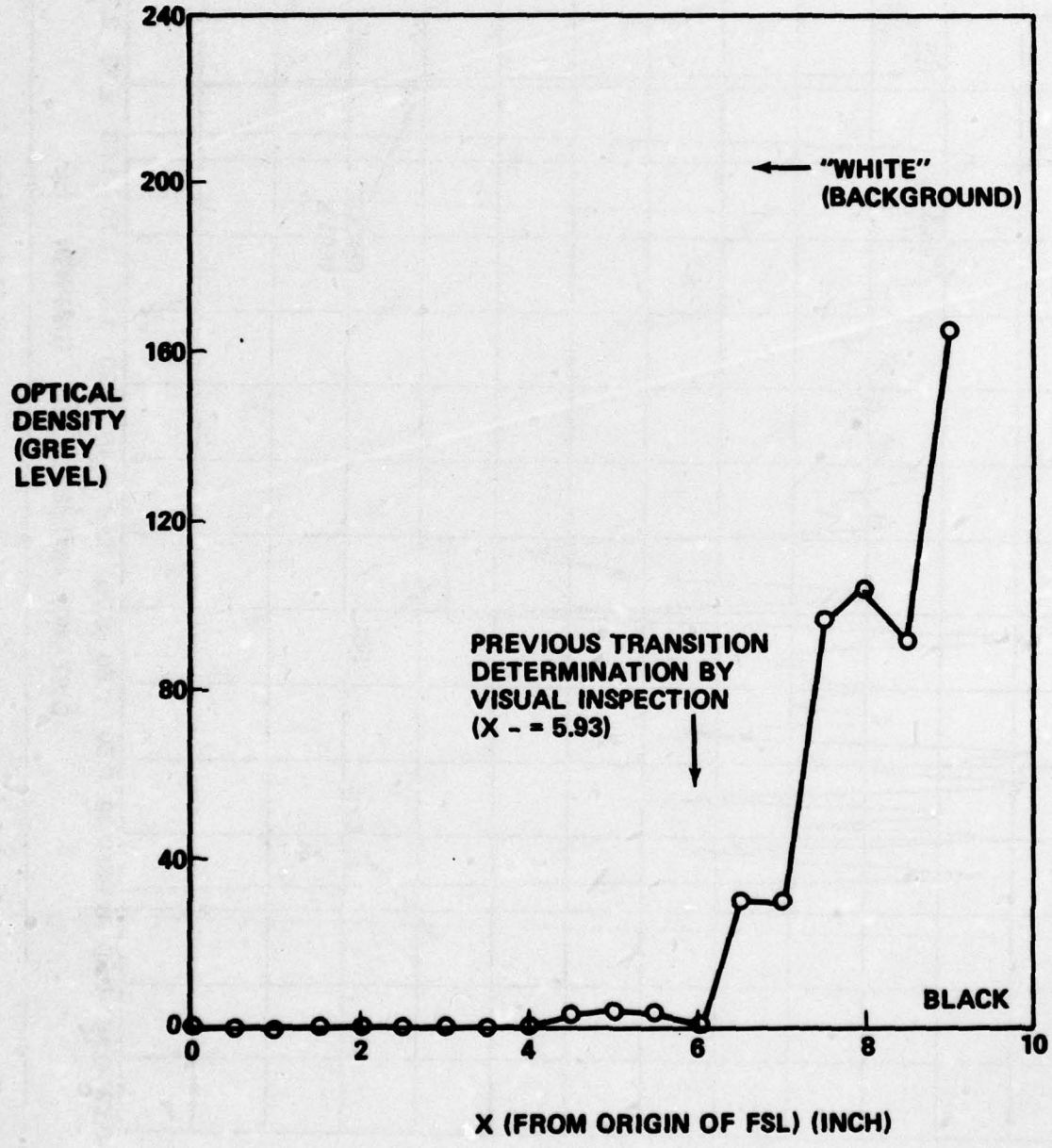

FIGURE 20. Comparison of transition detection between the densitometer and the visual methods.

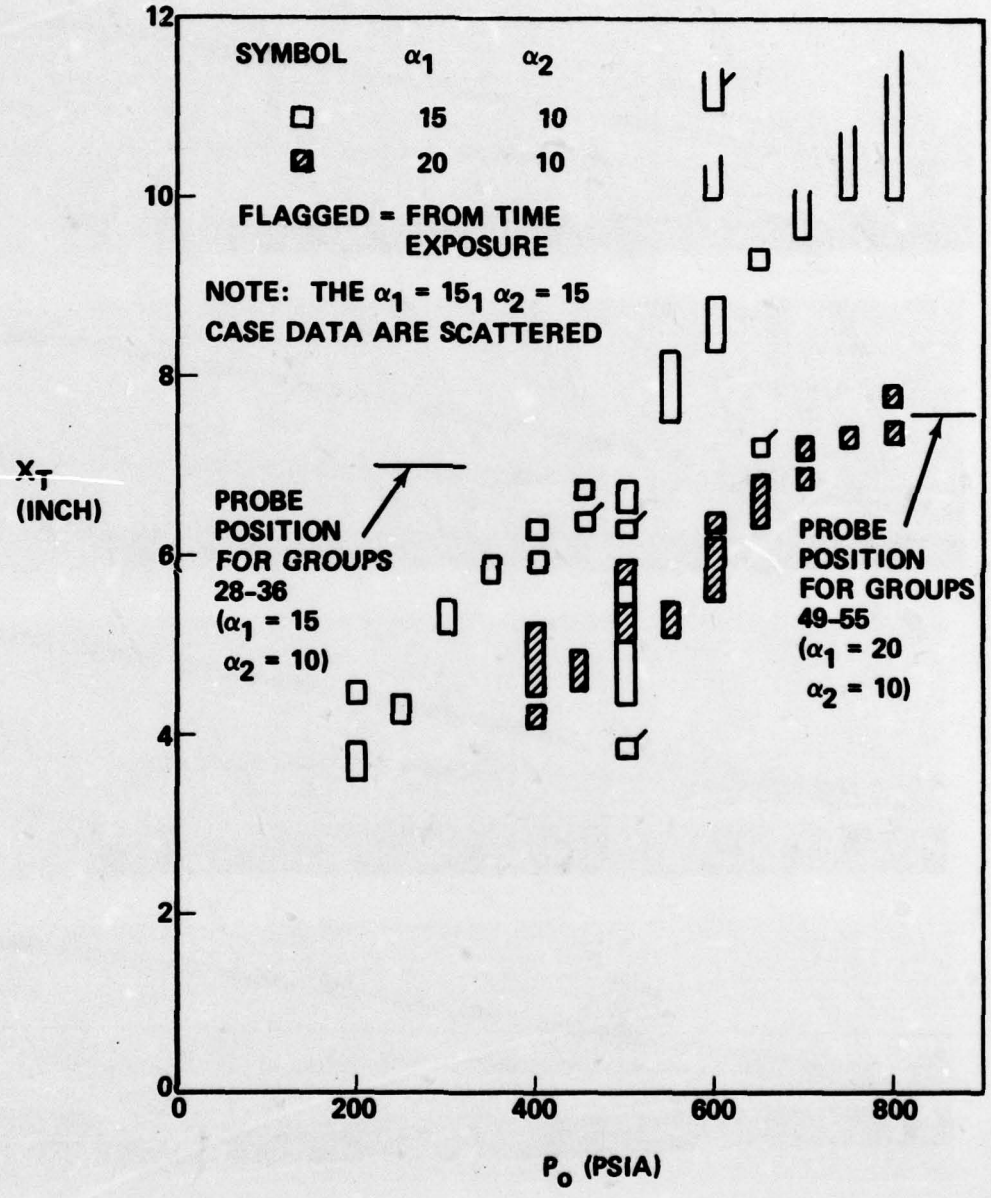

FIGURE 21. Variation of the transition distance with tunnel pressure.

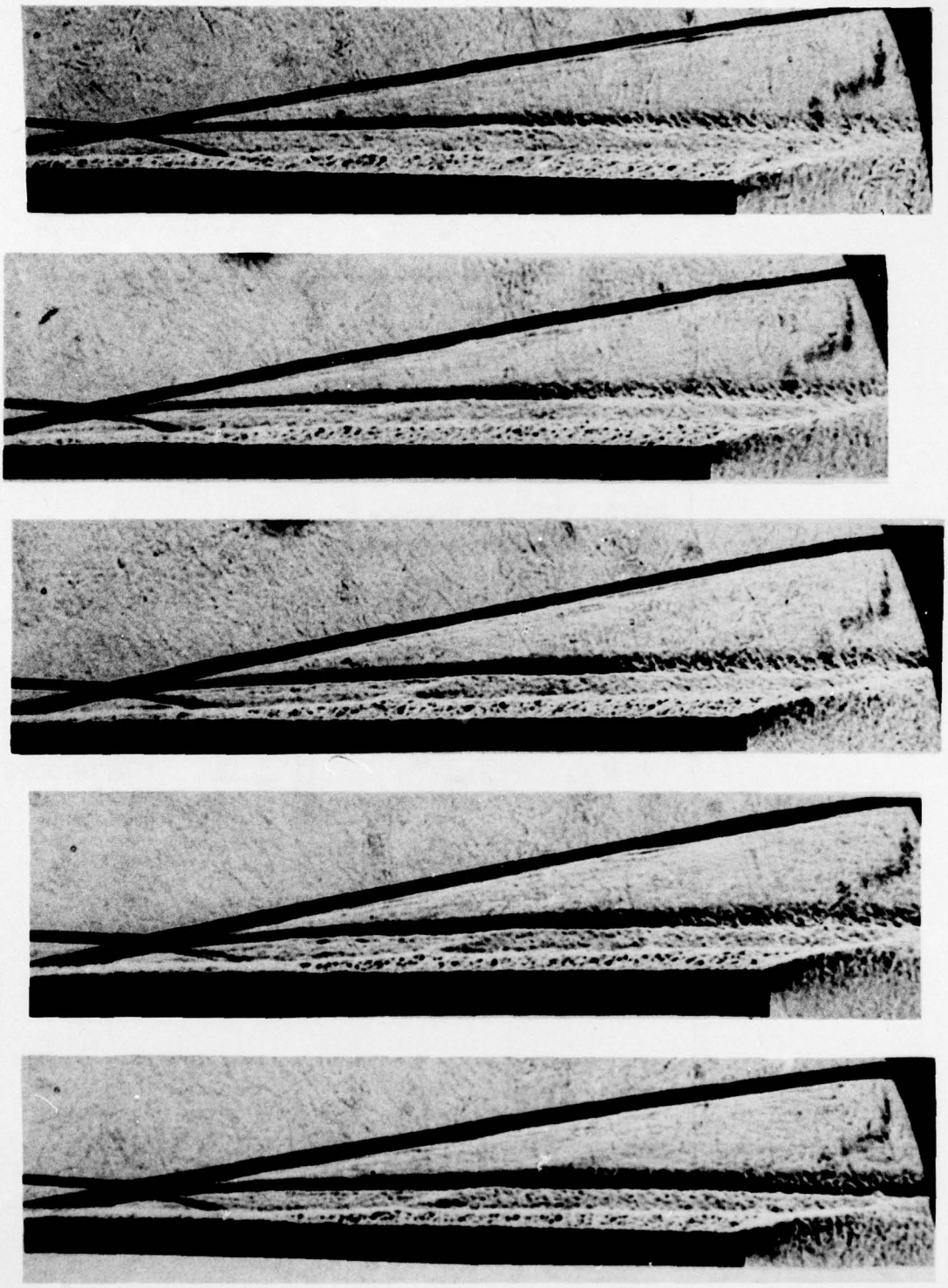

FIGURE 22. Shadowgrams of the free shear layer at (from top to bottom) 200, 300, 400, 500, and 600 psia.

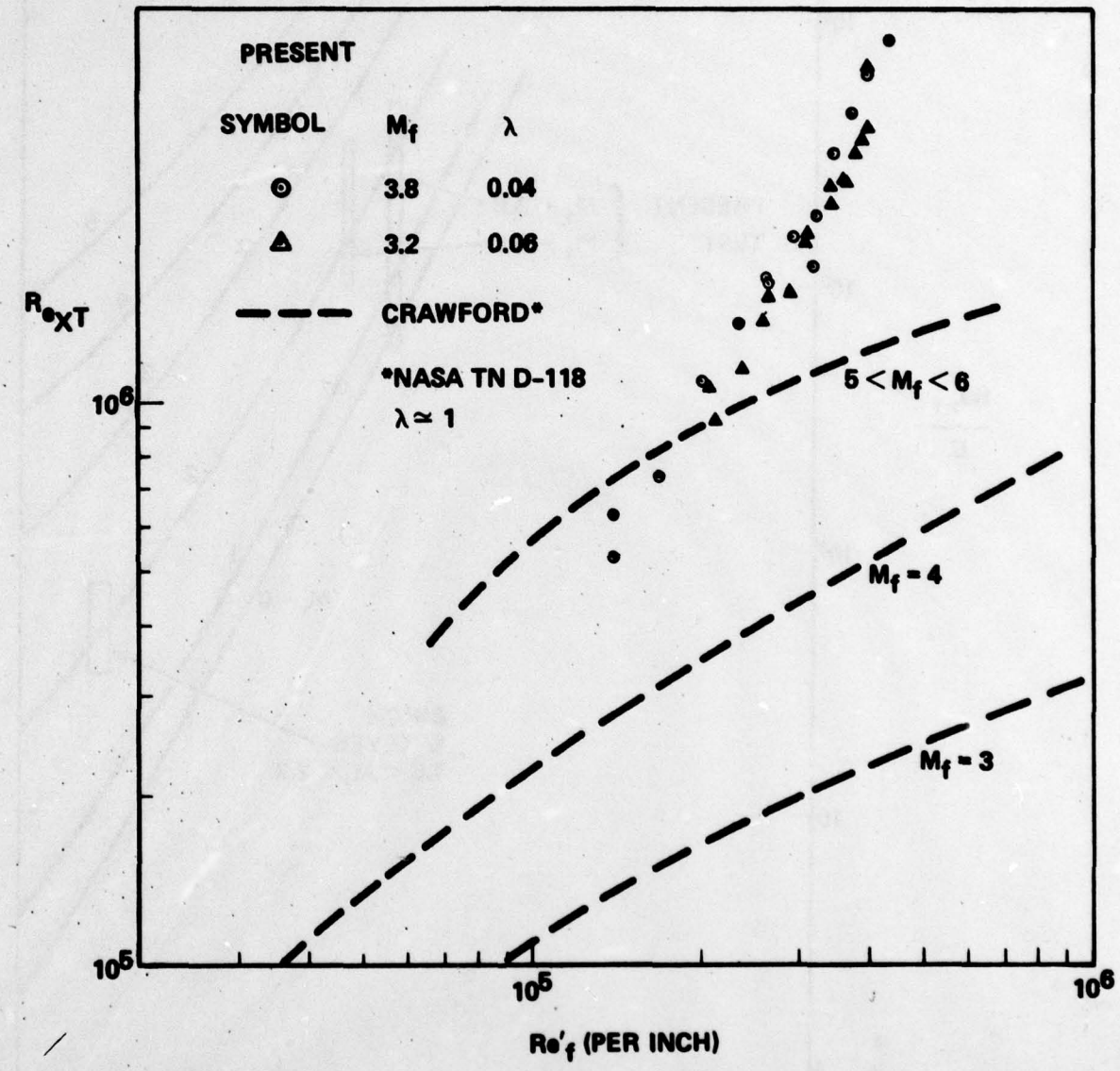

FIGURE 23. Variation of the measured transition Reynolds number with the unit Reynolds number.

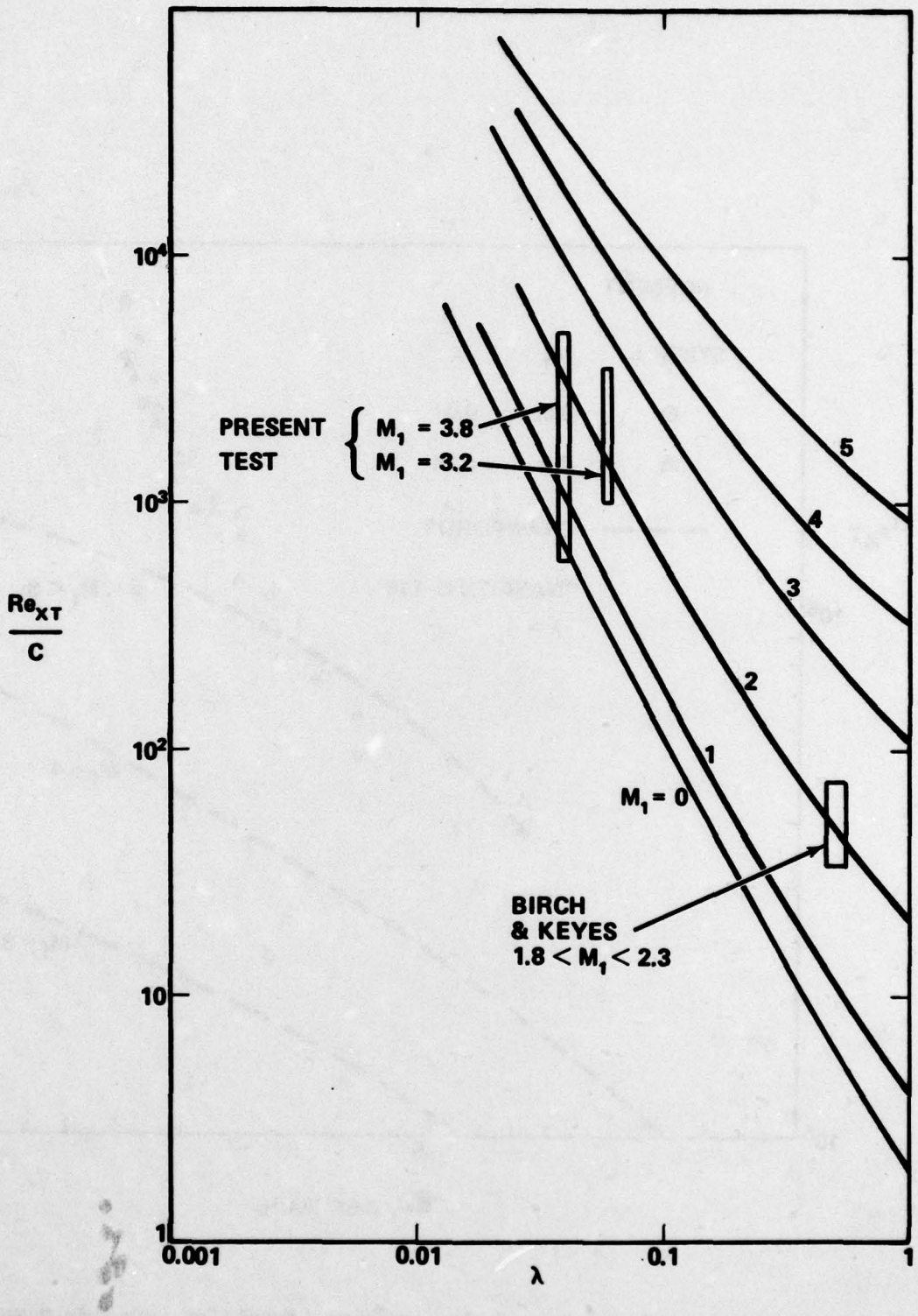

FIGURE 24. Comparison of the theory with the present data and the Birch and Keyes data.

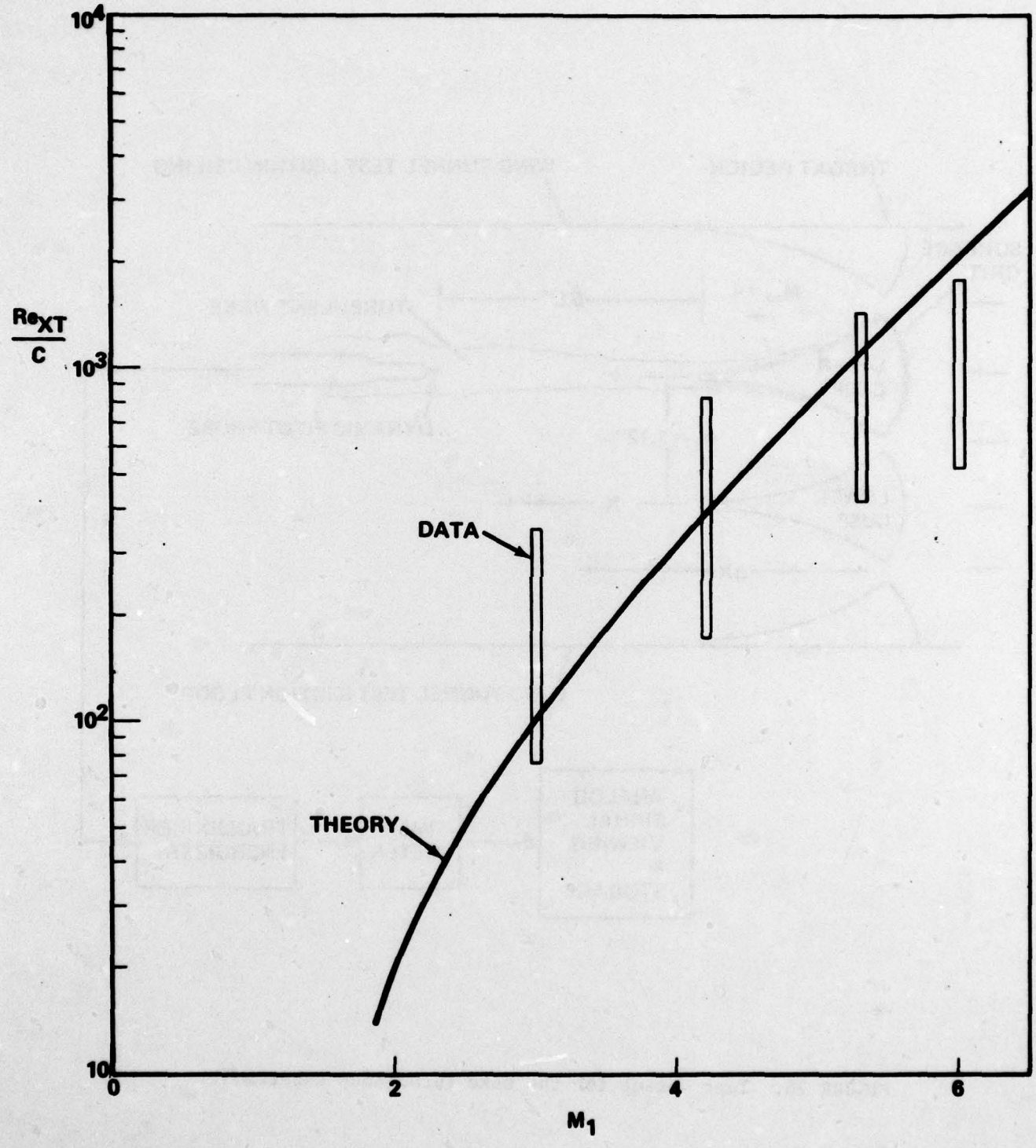

FIGURE 25. Comparison of the theory with Crawford's data.

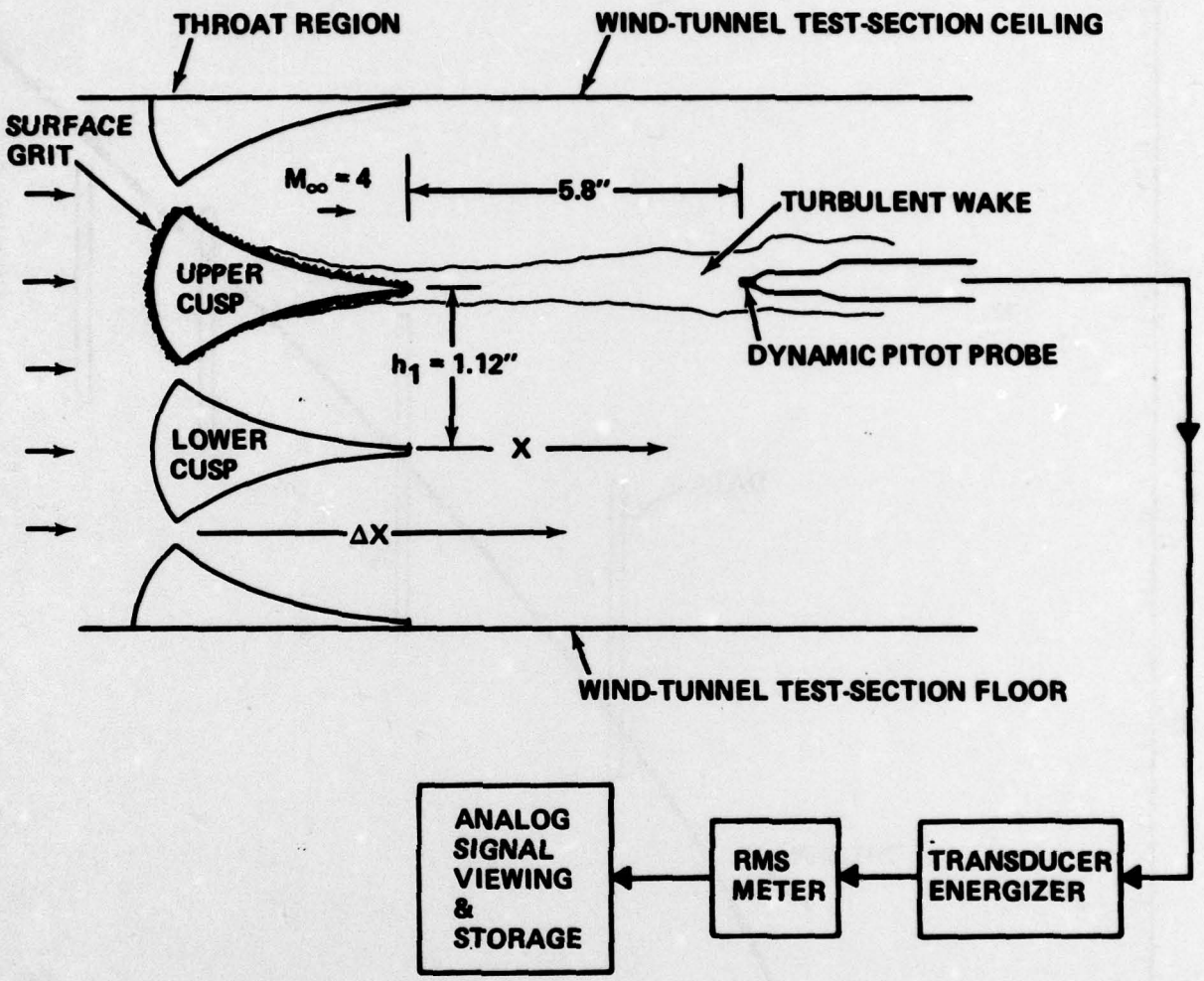

FIGURE 26. Test set-up for the wake turbulence experiment.

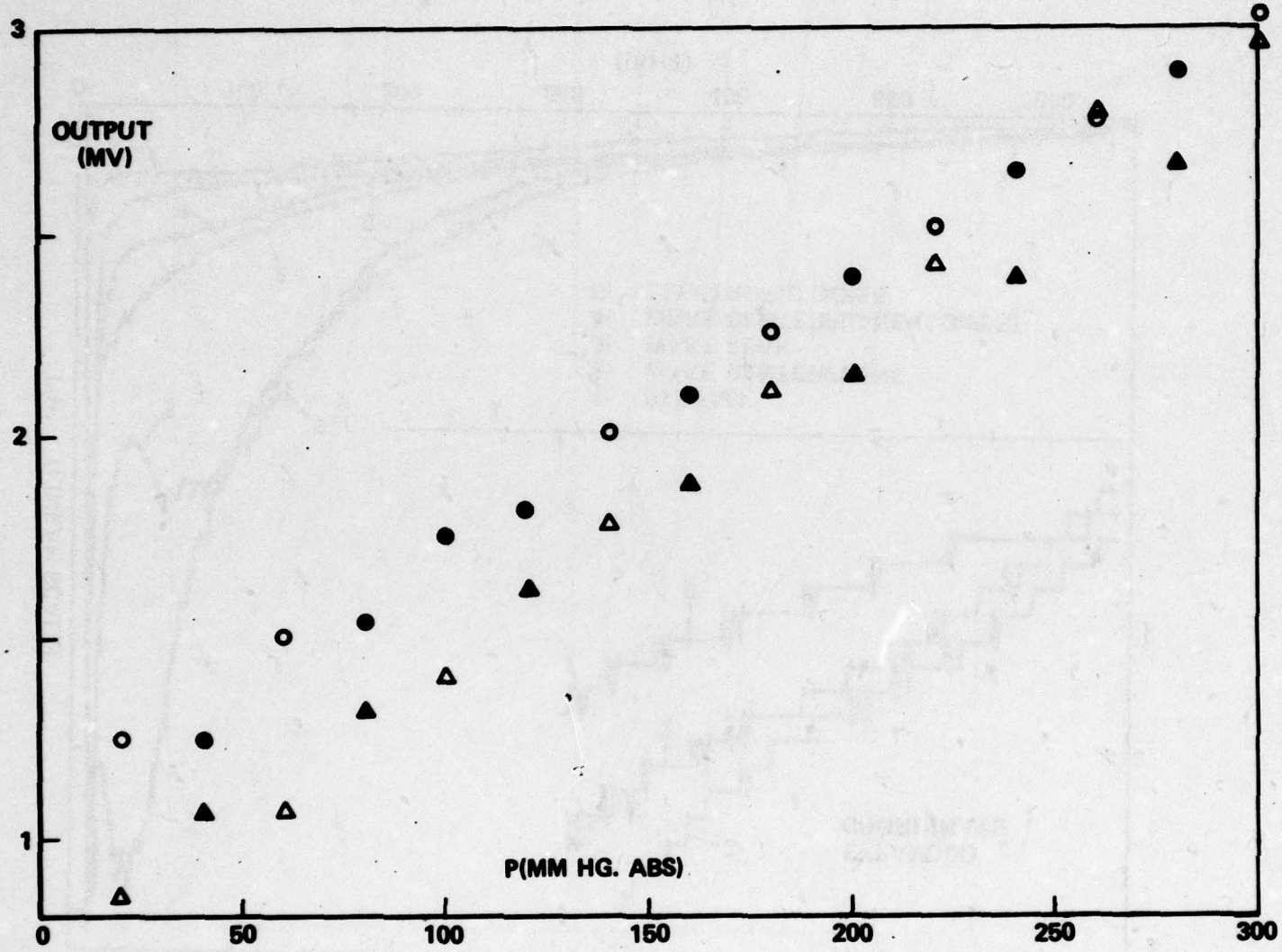

FIGURE 27. Calibration of the Kulite CQL-030-100 transducer. Different symbols represent four different calibrations.

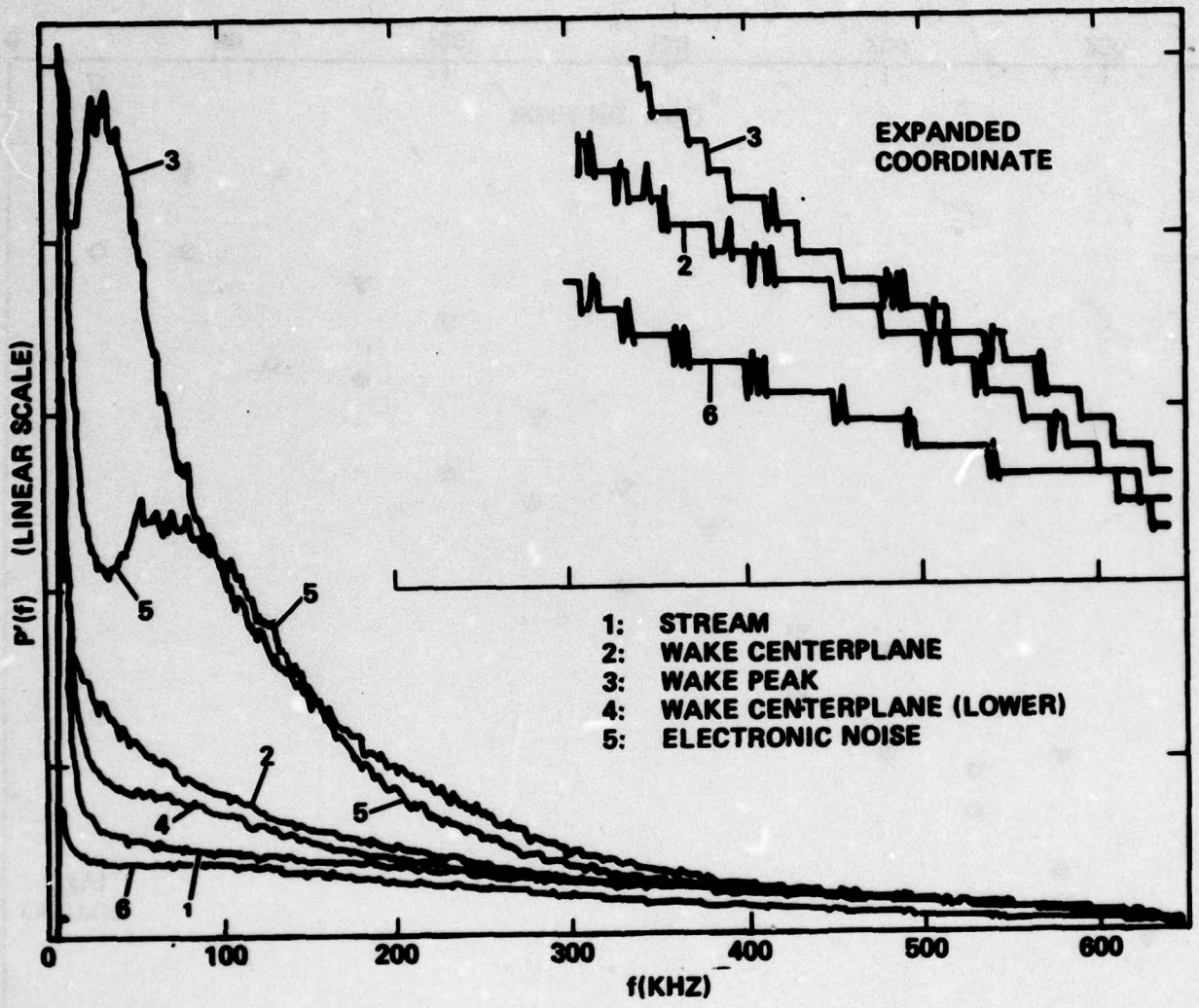

FIGURE 28. Spectra of the transducer output in the flow.

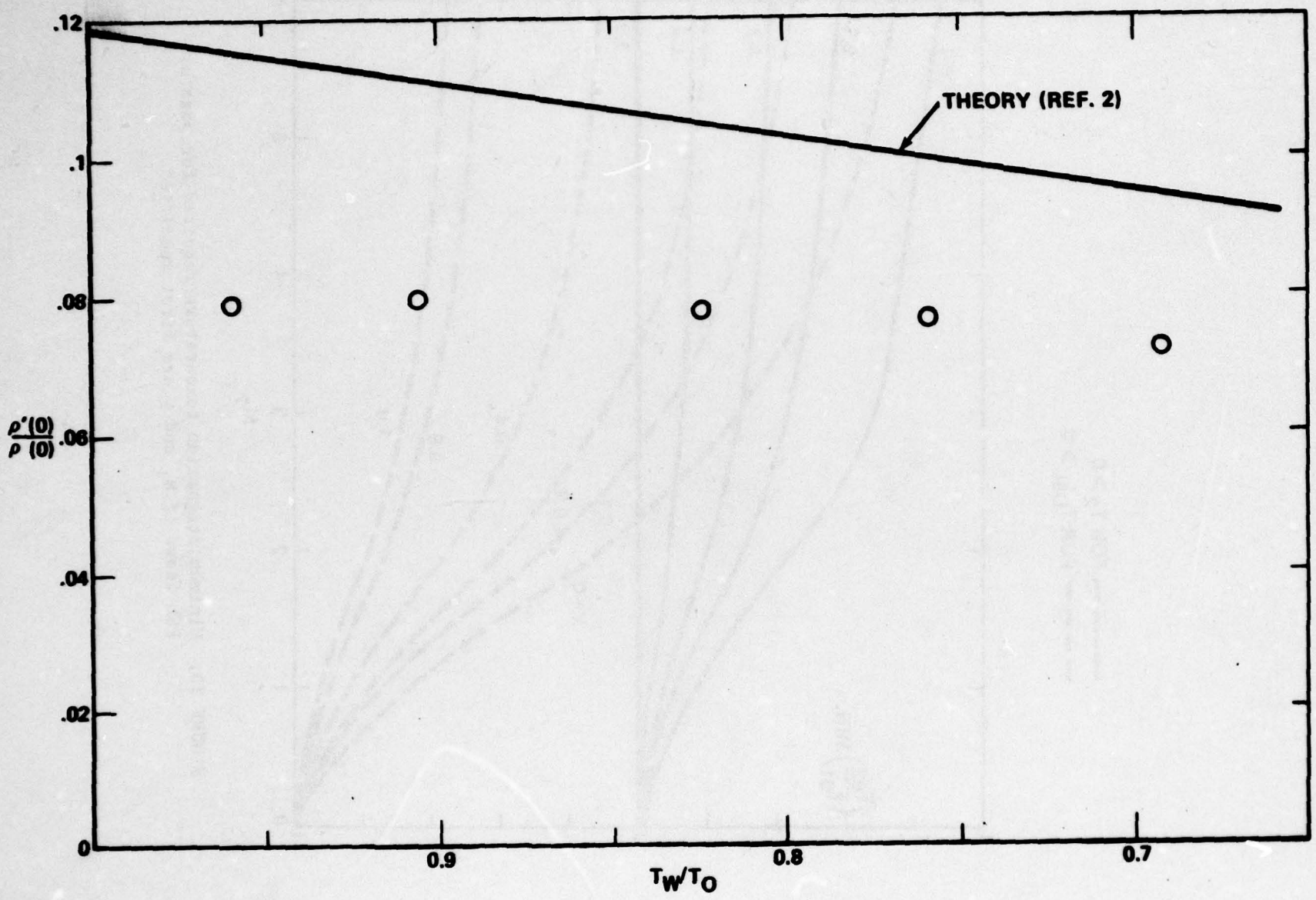

FIGURE 29. Comparisons of the ρ'/ρ measurements with the theory.

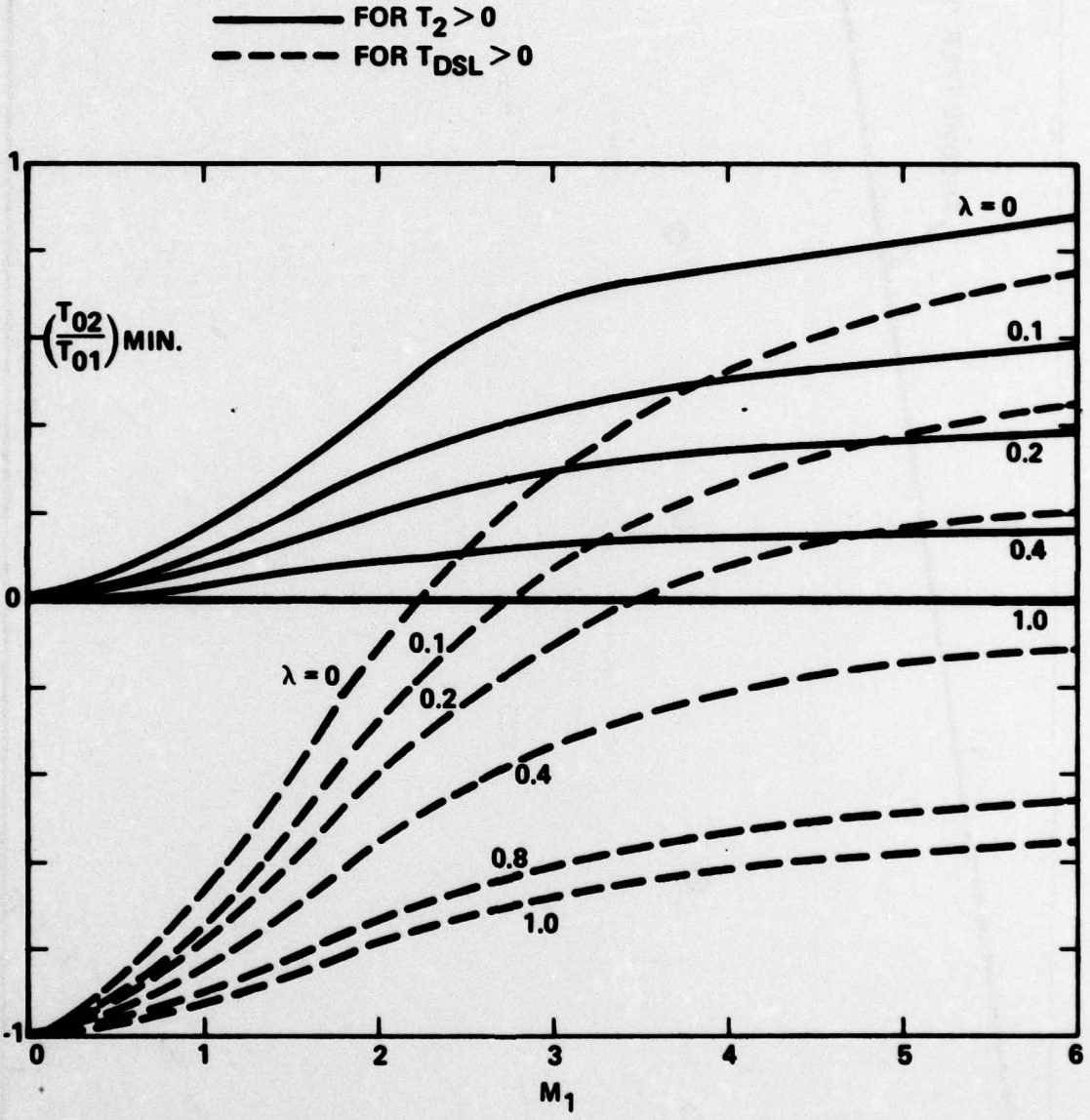

FIGURE 30. Minimum stagnation temperature required for possible FSL flows if M_1 and λ are first specified.

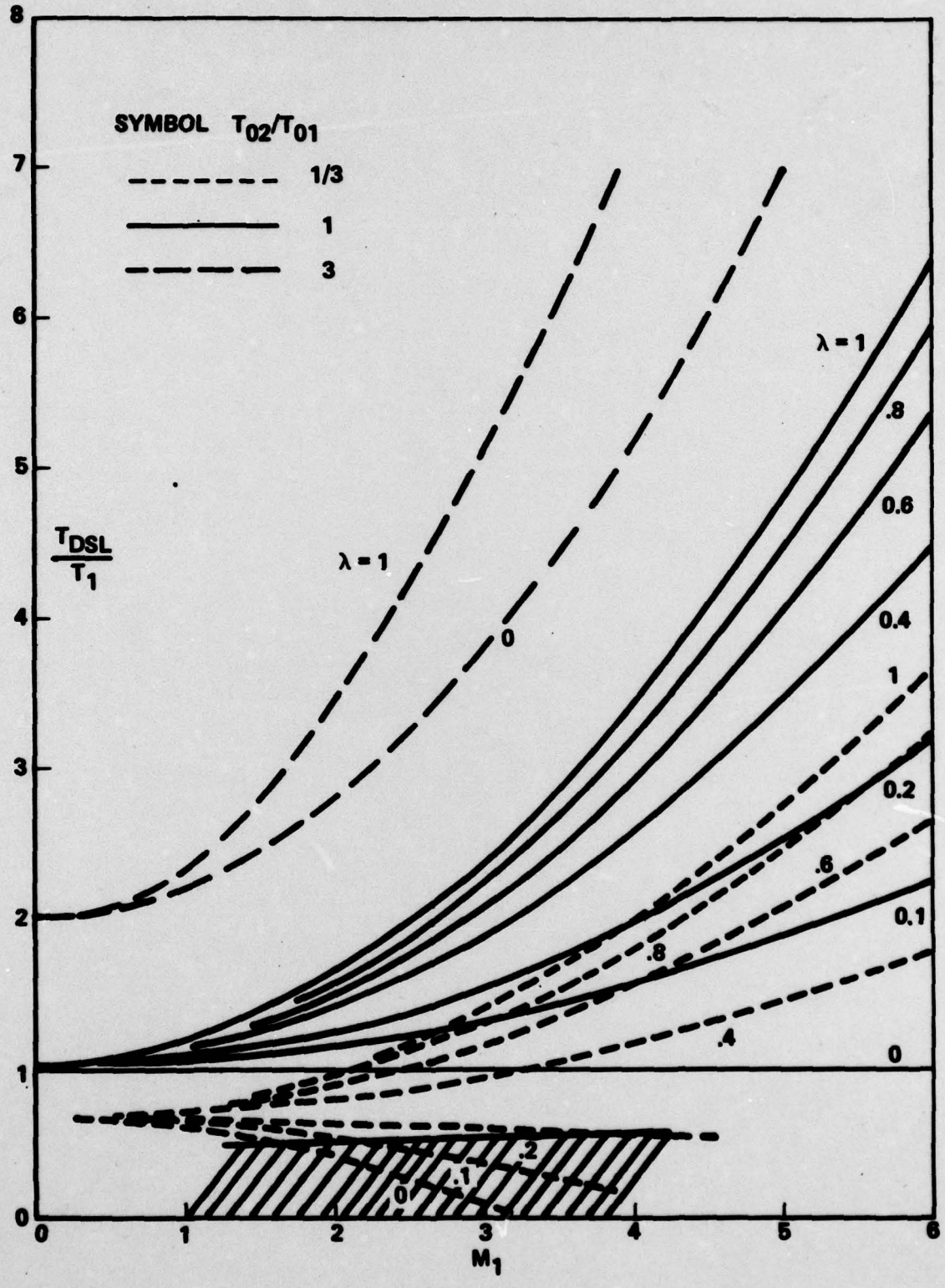

FIGURE 31. The DSL temperature according to the Crocco relation.

APPENDIX A

THE DIVIDING-STREAMLINE TEMPERATURE IN SHEAR LAYERS ACCORDING TO THE CROCCO RELATION

The objective of this Appendix is to derive an expression for the static temperature T_{DSL} on the dividing streamline, which accounts for Mach number and speed ratio variation from low to high levels, as well as arbitrary total temperature differences between the two streams. Excepting differences in molecular composition, this would then provide the information needed to encompass all conceivable physical ranges of free shear layers.

Our task is, actually, to simplify and exploit the temperature-velocity relation ("Crocco relation") derived by Shapiro (Ref. 24), Korst and Chow (Ref. 25) and others:

$$\frac{T-T_1}{T_1} = f(M_1)\left[1-\left(\frac{u}{u_1}\right)^2\right] + \left[\frac{1-\frac{T_2}{T_1}}{1-\frac{u_2}{u_1}} + f(M_1)\left(1+\frac{u_2}{u_1}\right)\right]\left(\frac{u}{u_1}-1\right) \qquad (A.1)$$

The objective here is to evaluate this formula at the dividing streamline (or "DSL"):

$$\frac{U_{DSL}}{u_1} = \frac{1}{2}\left(1+\frac{u_2}{u_1}\right) \qquad (A.2)$$

and express the result in terms of M_1, λ and T_{02}/T_{01}. Note that

$$f(M_1) = \frac{\gamma-1}{2} M_1^2 \qquad (A.3)$$

To do this, note that

$$T_1 = T_{01} - \frac{u_1^2}{2C_p} \qquad (A.4)$$

$$T_2 = T_{02} - \frac{u_2^2}{2C_p} \qquad (A.5)$$

Folding the latter two equations into (A.1) we obtain, after some algebra, the following two alternative equations:

$$\frac{T_{DSL}-T_1}{T_1} = f(M_1)\frac{\lambda^2}{(1+\lambda)^2} - \frac{1}{2}\left(1-\frac{T_2}{T_1}\right) \qquad (A.6)$$

$$\frac{T_{DSL} - \bar{T}}{T_1} = f(M_1) \left(\frac{\lambda}{1+\lambda}\right)^2 \qquad (A.7)$$

with

$$\bar{T} = \frac{T_1 + T_2}{2} \qquad (A.8)$$

These equations are still unsatisfactory because they do not contain the ratio T_{02}/T_{01} explicitly; further manipulation produces the desired result:

$$\frac{T_{DSL}}{T_1} = \frac{1}{2}\left(1 + \frac{\gamma-1}{2} M_1^2\right)\left(1 + \frac{T_{02}}{T_{01}}\right) - \frac{(\gamma - 1) M_1^2}{2(1+\lambda)^2} \qquad (A.9)$$

In equation (A.9) the parameters M_1, λ and T_{02}/T_{01} are independent, and any set of them should define a unique T_{DSL}/T_1 value. Physically speaking, however, there is an exception made when the second term on the r.h.s. of (A.9) exceeds the first which, it will be noted, can happen especially if $T_{02}/T_{01} << 1$. In this case $T_{DSL} < 0$, a clearly impossible (but algebraically permitted) result. There are, therefore, minimum allowed values of T_{02}/T_{01} which, combined with any pair of prescribed M_1,λ values, will give $T_{DSL} > 0$ according to (A.9), and these are plotted in Figure 30. An additional, but similar restriction on T_{02}/T_{01} arises when we require that in the hypothesized "slow" stream (subscript "2") the temperature $T_2 > 0$. This criterion can be derived from Eq. (A.7) and (A.8) and is plotted on the same figure. The criterion required to keep $T_2 > 0$ is, as Figure 30 shows, more restrictive than the requiring $T_{DSL} > 0$; that is, the latter criterion can be ignored so long as the former is accounted for. Thus, according to Figure 30, if we hypothesize a FSL with $M_1 = 3$ and $\lambda = 0.1$, say, then we can prescribe to this flow any T_{02}/T_{01} larger than 0.42 or so. Values of T_{02}/T_{01} less than that will create a physically unattainable flow. Thus, Equation (A.9) subject to the restrictions of Figure 30 is the necessary tool for computing the kinematic viscosity entering the transition formula in the text.

We will forego demonstrating the lateral variation of temperature across the FSL according to (A.1), since such plots are relatively easy to do. It is, however, important to keep in mind that there are values of T_{02}/T_{01} for which T does not vary monotonically from T_1 to T_2. This can be seen by noting that

$$\frac{T_2}{T_1} = \left[1 + \frac{\gamma-1}{2} M_1^2\right] \frac{T_{02}}{T_{01}} - \frac{\gamma-1}{2} M_1^2 \left(\frac{1-\lambda}{1+\lambda}\right)^2 \qquad (A.10)$$

and plotting $(T-T_1)/T_1$ vs. η, where as usual:

$$\frac{u}{u_1} = \frac{1}{1+\lambda}\left[1 + \lambda \cos \eta\right] \qquad (A.10)$$

The result will show that, especially for large M_1 and λ and for $T_{02}/T_{01} < 1$, T arrives at a maximum between the two streams. The physical reason, of course, is that as the fast stream slows down to match the speed of the slow one, it experiences an isentropic temperature rise. In such cases the temperature profile resembles, as it should, a cold-wall supersonic boundary layer.

This parenthetic remark was made to prepare the user of Eq. (A.9) for occasional "odd" behavior of T_{DSL}, such as an actual decrease for certain conditions illustrated on Figure 31 on which Eq. (A.9) is plotted. Such behavior, setting in for $T_{02}/T_{01} < 1$, will have consequences in the transition predictions found in that text.